NTNU – Trondheim
Norwegian University of
Science and Technology

# Loads on the Gravity-net-cage from Waves and Currents

Ida Håøy Grue

Marine Technology
Submission date: June 2014
Supervisor: Sverre Steen, IMT
Co-supervisor: Arne Fredheim, SINTEF fiskeri og havbruk

Norwegian University of Science and Technology
Department of Marine Technology

**NTNU Trondheim**
**Norwegian University of Science and Technology**
*Department of Marine Technology*

# MASTER THESIS IN MARINE TECHNOLOGY

## SPRING 2014

## FOR

## Ida Håøy Grue

## Loads on the Gravity-net-cage from Waves and Currents

Due to a lack of suitable locations in sheltered waters, and due to environmental concerns there is a drive to locate salmon fish farms in more exposed locations. In such locations, wave loads will be more important relative to current loads. In order to dimension new fish farms, and to check new designs it is important to have reliable software tools for prediction of the dimensioning loads from waves and current. The starting point for this thesis is a model test campaign in the large ocean basin at the Marine Technology Centre in Trondheim, where a model of a floating fish cage was tested in various combinations of waves and current.

The aims of this thesis are to contribute to identify critical conditions by investigating the mooring line loads of the experiments, and to validate simulations with the code FHsim.

It is expected that the thesis shall cover the following topics

- A review and analysis of the model test, including presentation of the most important results that are used in the validation.
- A presentation of the simulation code subject to validation, including a summary of the theory it is built on.
- Results of the validation study, including discussion of possible reasons for significant deviations between experiment and simulations.
    - Here it might be appropriate to discuss what is a "significant deviation", and also the quality and accuracy of the experimental results.

In the thesis the candidate shall present her personal contribution to the resolution of problem within the scope of the thesis work.

Theories and conclusions should be based on mathematical derivations and/or logic reasoning identifying the various steps in the deduction.

The thesis work shall be based on the current state of knowledge in the field of study. The current state of knowledge should be established through a thorough literature study, the results of this study shall be written into the thesis. The candidate should utilize the existing possibilities for obtaining relevant literature.

**NTNU Trondheim**
**Norwegian University of Science and Technology**
*Department of Marine Technology*

The thesis should be organized in a rational manner to give a clear exposition of results, assessments, and conclusions. The text should be brief and to the point, with a clear language. Telegraphic language should be avoided.

The thesis shall contain the following elements: A text defining the scope, preface, list of contents, summary, main body of thesis, conclusions with recommendations for further work, list of symbols and acronyms, reference and (optional) appendices. All figures, tables and equations shall be numerated.

The supervisor may require that the candidate, in an early stage of the work, present a written plan for the completion of the work. The plan should include a budget for the use of computer and laboratory resources that will be charged to the department. Overruns shall be reported to the supervisor.

The original contribution of the candidate and material taken from other sources shall be clearly defined. Work from other sources shall be properly referenced using an acknowledged referencing system.

The thesis shall be submitted electronically (pdf) in DAIM:

- Signed by the candidate
- The text defining the scope (signed by the supervisor) included
- Computer code, input files, videos and other electronic appendages can be uploaded in a zip-file in DAIM. Any electronic appendages shall be listed in the main thesis.

The candidate will receive a printed copy of the thesis.

Supervisor : Professor Sverre Steen
Advisors: Arne Fredheim and Trygve Kristiansen
Start : 14.01.2014
Deadline : 10.06.2014

Trondheim, 14.01.2014

Sverre Steen
Supervisor

# Abstract

Due to limited space close to shore and environmental concerns, the trend has become to move the fish farms to more exposed areas. This motivates the study of loads on the fish farm in more energetic currents and waves.

In this thesis the conventional gravity net cage is analysed from an experimental and numerical point of view. The focus is on mooring line loads, which represent the global loads acting on the system. The numerical program FhSim, which is SINTEF Fisheries and Aquaculture inhouse software, is subject for a comparison study in terms of mooring line loads. Two systems of the gravity net cage are analysed.

Experiments conducted by MARINTEK in May 2013 are analysed to investigate the mean load features in large current and waves. The results are compared to mean load predictions from the numerical code FhSim. A comparative study between FhSim and the numerical code developed by Kristiansen & Faltinsen (2014) is also performed.

Experimental analysis in irregular waves and currents show that the mean mooring line load is dominated by current. The mean load is found to increase with increased wave height and wave period. These trends are captured by the numerical programs. The mean load in currents and waves is decomposed into a static load which is the current only contribution, and the remaining dynamic force part. Alternative scalings of the mean dynamic force included $(\frac{u_w}{U_\infty})^2$ and $\zeta_a^2$.

From the comparative study, it is found that FhSim predicts the mean loads with a reasonable agreement in a combination of the current velocity U=0.5m/s and the wave steepness of H/$\lambda$=1/30. In a combination of larger currents and steeper waves, FhSim overestimates the mean load for

the studied model. This can be explained by the implemented Morison load model and the increased water flow velocity across the net.

In the analysis of a complete mooring line system, a prediction error was detected in the numerical program FhSim. Together with the possible overestimation of mean mooring line loads in large currents and waves this must be accounted for when assessing mooring line loads by use of FhSim.

In a comparison study, a set of high accuracy data from both numerical predictions and experimental measurements should be ensured. A reduction of systematic errors and detection of precision errors improves the quality of the data. In order to confirm the observed features regarding mean load predictions from FhSim, further investigations with a wider range of experimental test conditions in large currents and waves are required.

# Sammendrag

Det begynner å bli færre tilgjengelige lokaliteter for havbruk i kystnære strøk, og det forventes at fiskemerdene vil bli flyttet lenger til havs. Dette gir grunnlag for å undersøke miljølaster på fiskemerden i store strømhastigheter og større bølger.

I denne masteroppgaven blir den konvensjonelle fiskemerden analysert med eksperimentelle forsøk og numeriske verktøy. Fokuset i analysen er på oppankringskreftene, siden ankerlinene representerer de globale kreftene på fiskemerden. I oppgaven blir det numeriske verkøyet FhSim anvendt i et sammenlikningsstudium. FhSim er utviklet av SINTEF Fiskeri og Havbruk. To forskjellige konfigurasjoner av oppankringsdesign blir studert.

I mai 2013 gjennomførte MARINTEK et forsøk av en konvensjonell fiskemerd. Resultatene fra eksperimentet blir analysert og egenskapene til gjennomsnittskraften i ankerlinene undersøkt under miljøpåvirkning fra stor strøm og bølger. Resultatene blir sammenliknet med beregninger av gjennomsnittskraft fra FhSim. Det utføres også et sammenlikningsstudium mellom FhSim og den numeriske koden utviklet av Kristiansen & Faltinsen (2014).

I irregulær sjø og strøm viser de eksperimentelle resultatene at størsteparten av gjennomsnittskraften i oppankringslinene skyldes påvirkingen fra strøm. Gjennomsnittskraften øker med økende bølgehøyde og bølgelengde. Begge de numeriske verktøyene gjenskaper disse trendene. Gjennomsnittskraften blir dekomponert i en statisk last som skyldes kraftbidraget fra kun strøm, og i et dynamisk kraftbidrag som skyldes både bølger og strøm. Alternative skaleringer for den dynamiske gjennomsnittskraften inkluderer $(\frac{u_w}{U_\infty})^2$ og $\zeta_a^2$.

Fra sammenlikningsstudiet ser man at FhSim beregner gjennomsnittskraft med god overestemmelse under ytre påvirkning fra en strøm med hastighet

U=0.5m/s og bølger med steilhet H/$\lambda$=1/30. Med påvirkning fra sterkere strøm og steilere bølger overestimerer FhSim gjennomsnittskraften. Dette funnet kan forklares med den implementerte lastmodellen som er av Morison type, og den økte hastigheten til vannstrømmen gjennom nettet.

Det ble oppdaget en presisjonsfeil i den numeriske koden under analysen av fiskemerden med komplett oppankringsystem. Dette må tas i betraktning sammen med overestimeringen av oppankringskraft dersom FhSim skal brukes til dimensjonering av ankerliner.

I et sammenlikningsstudium kreves det et datasett med stor nøyaktighet i både de eksperimentelle målingene og de numeriske beregningene. Det er nødvendig å redusere systematiske feil og presisonsfeil for å få data med høy kvalitet. For å bekrefte funnene for oppankringskraft predikert fra FhSim, bør det gjøres flere simuleringer i stor strøm og bølger med et bredere eksperimentelt datasett som sammenlikningsgrunnlag.

# Preface

This master thesis is written during the spring 2014 as a part of the studies for the Master of Science degree in Marine Technology at the Norwegian University of Science and Technology (NTNU) in Trondheim. The thesis is written in collaboration with SINTEF Fisheries and Aquaculture.

I am grateful to my supervisor, Professor Sverre Steen, for help and advices in meetings throughout the semester. Guiding and discussions with my advisors Trygve Kristiansen at MARINTEK and Arne Fredheim at SINTEF Fisheries and Aquaculture have inspired me in the work. I am very thankful for the assistance I have received from Per Christian Endresen at SINTEF Fisheries and Aquaculture and I want to thank Håvard Holm for computer assistance connected to the applied numerical code.

I would also like to thank my fellow students, for valuable discussions and giving feedback in the writing process. Finally, I would like to thank my family for their never ending support.

Trondheim, $10^{th}$ of June 2014
Ida Håøy Grue

# Contents

# List of Figures

# List of Tables

# Nomenclature

## General comments

- Symbols and abbreviations are generally defined the first time they appear in the text.
- Only the most important symbols are defined here
- A symbol may be given several meanings.

## Roman letters

| | |
|---|---|
| $A$ | Projected area |
| $C_D$ | Drag force coefficient |
| $C_D^0$ | Drag coefficient for net cage in initial configuration in calm water |
| $C_D^{circ.cyl.}$ | Reynolds number dependent drag coefficient |
| $C_L$ | Lift force coefficient |
| $C_N$ | Normal force coefficient |
| $C_T$ | Tangential force coefficient |
| $D$ | Diameter of the net cage |
| $D_x$ | Diameter of the structural part x |
| $d_w$ | Twine diameter |
| $F_D$ | Drag force |

| | |
|---|---|
| $F_{DYN}$ | Dynamic mean force |
| $F_L$ | Lift force |
| $F_{TOT}$ | Total mean force |
| $F_{STATIC}$ | Static mean force |
| $f_u$ | Upper cut-off frequency |
| $g$ | Gravity constant |
| $Hs$ | Significant wave height |
| $H$ | Wave height |
| $k$ | Wave number |
| $l_w$ | Twine length |
| $L$ | Depth of cylindrical part of net cage |
| $N$ | Number of samples |
| $P_X$ | Precision limit |
| $r$ | velocity reduction factor |
| $Rn$ | Reynolds number |
| $Sn$ | Solidity ratio |
| $S_X$ | Standard deviation of a sample |
| $T$ | Wave period |
| $Tp$ | Peak period |
| $u_j$ | Velocity of the net cage |
| $u_w$ | Wave particle velocity |
| $U$ | Current velocity |
| $U_\infty$ | Ambient far field current velocity |
| $U_{rel}$ | Relative velocity |
| $U_S$ | Characteristic cross flow water velocity at the twines |
| $\overline{X}$ | Ensemble average |

# Greek letters

| | |
|---|---|
| $\epsilon$ | Constant wave steepness |
| $\lambda$ | Wave length |
| $\lambda_p$ | Characteristic wave length |
| $\nu$ | Kinematic viscosity of water |
| $\omega$ | Wave frequency |
| $\rho$ | Water density |
| $\theta$ | Angle of attack |
| $\sigma_{AW}$ | Coefficient for added drag |
| $\zeta_a$ | Wave amplitude |

# Abbreviations

| | |
|---|---|
| AL | Anchor line |
| C1 | Current only condition, U=0.5 m/s |
| C2 | Current only condition, U=0.7 m/s |
| CW1 | Combined current and regular wave condition, H=2.5m, T=6.0s, U=0.5m/s |
| CW2 | Combined current and regular wave condition, H=2.5m, T=8.0s, U=0.5m/s |
| UN | Uncertainty |
| W1 | Regular wave condition, H=2.5m, T=6.0s |
| W2 | Wave only condition, H=2.5m, T=8.0s |

# Chapter 1

# Introduction

Aquaculture food production is increasing in proportions all over the world. Driving forces are population growth, stresses on the fresh water resources, employment and uncertainty associated with wild fish stocks (Shainee et al. 2013). Due to limited space in near shore areas and environmental concerns, it is expected that future aquaculture production sites will be located further from shore. This motivates the study of the hydrodynamic forces acting on the structure and its dynamical behaviour in more energetic current and waves.

## 1.1 Background

There is an unreleased potential within aquaculture. Since most of the world's wild fish stocks are fully exploited, and the land resources limited, aquaculture has to constitute a part of the future growth in food production.

By definition, aquaculture is *"the farming of aquatic organisms in inland and coastal areas, involving intervention in the rearing process to enhance production and the individual or corporate ownership of the stock being cultivated"* (FAO, 2012).

In the process of designing a fish farm, factors concerning the fish, the fish farmer and the society have to be considered (Shainee et al. 2013). From a structural point of view, the sea loads and response are the the main concerns.

One must also bear in mind that the aim of the structure is fish growth, and account for the presence of the living fish and the practice of surveillance for the fish farmer. In such a way, the aquastructure design can be considered as a compromise between optimized technology, the fish's welfare, the fish farmer's access and the society's requirements (Shainee et al. 2013).

Throughout the history, fishery has been a major industry in Norway. With a location providing optimal climate conditions and a long stretched coast line, there are many sites well suited for aquaculture food production. A consequence of the rapid increase in food production have been enlargement of the net cages. Utilization of the conventional gravity net cage have been stretched to the limit regarding maximum fish content and environmental conditions at the exposed sites. The conventional aquaculture structure design might soon have reached the limit of enlargement. It is a question of time before new and more robust designs are released in the aquaculture industry. However, use of the conventional net cage is expected to continue due to its cost effectiveness.

Currently, the conventional gravity net cage is widely used for aquaculture production. Moving the conventional net cage to sites with adverse environmental conditions creates new scenarios and more frequent critical conditions. Increased impact from current leads to excess deformation of the net. Larger waves may cause challenges connected to operation and daily duties. Total global loads will increase, exerting larger loads on the mooring system. To ensure structural integrity and safe operation, analyses are required.

Structural failure and fish escape are issues of concern, due to economical losses and worries for biodiversity. The industry operates with a target goal of zero escapes and a wide ranging effort have been made to achieve it. Research and structural analysis have been performed and certification rules for fish farms have been established. After introduction of the Norwegian Technical Standard (NS 9415) through Norwegian legislation on April $1^{st}$ 2004, a dramatic reduction in fish escape was seen (Jensen et al. 2006). It describes the requirements for site survey, risk analysis dimensioning and design.

## 1.2 Scope and limitations

In this thesis a conventional gravity net cage is analysed by experiments and numerical simulations. The focus is on mooring line force, representing the global loads acting on the system. The applied environmental conditions can be considered as a combination of large currents and waves.

Two systems of the same gravity net cage are considered. The reason for analysing two systems of the gravity net cage, is that the systems have advantages and limitations in terms of available experimental data, model complexity and specifications of the available numerical programs.

From the analysis of experiments, a basic understanding of the mean load features are obtained. In order to validate FhSim, the experimental results are compared to the simulations. Simulations from FhSim is also compared to a second numerical code.

To determine the total mooring line load, the sum of amplitude and mean force should be considered. However, the main focus in this thesis is on the mean mooring line load.

## 1.3 Structure of the thesis

Chapter 2 gives an introduction to the structural parts comprising the gravity net cage. An overview of the environmental loads acting on the structure are presented.

Chapter 3 describes the mathematical model of the floater and net cage.

Chapter 4 outlines the organization of the two applied simulation softwares. FhSim is SINTEF Fisheries and Aquacultures inhouse software. The second program is the numerical code developed by Kristiansen & Faltinsen (2012*b*), which is denoted fishFarm in this thesis.

Chapter 5 describes the methodology of the performed work. A description of the two analysed gravity net cage systems is given.

Chapter 6 presents the analysis of an experiment executed in the ocean basin at MARINTEK in May 2013. The features of the mean mooring line loads of the gravity net cage are studied.

Chapter 7 presents a comparison study of the numerical program FhSim in large currents and waves. Experimental and simulated results of the similar setup as described in chapter 6 are compared. Additionally, Numerical results from FhSim and fishFarms are compared for a second gravity net cage model.

Chapter 8 concludes the results and in chapter 9 suggestions for further work are presented.

# Chapter 2

# Aquaculture net cages - an overview

A brief overview of some of the most important structures used in the aquaculture industry is presented. The floating fish farm typically consists of several net cages gathered in a configuration as shown in figure 2.1.

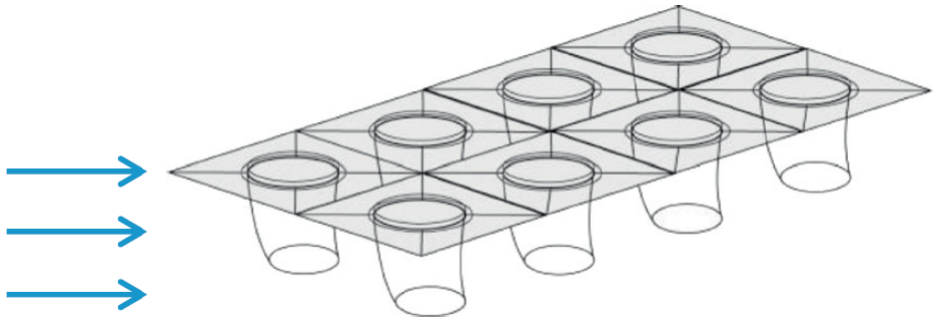

Figure 2.1: Configuration of a fish farm (Klebert et al. 2013)

## 2.1 The gravity net cage

The aquaculture structure consists of a net cage and a mooring system. The conventional design and dominant net cage type today is the gravity net cage

and is illustrated in figure 2.2.

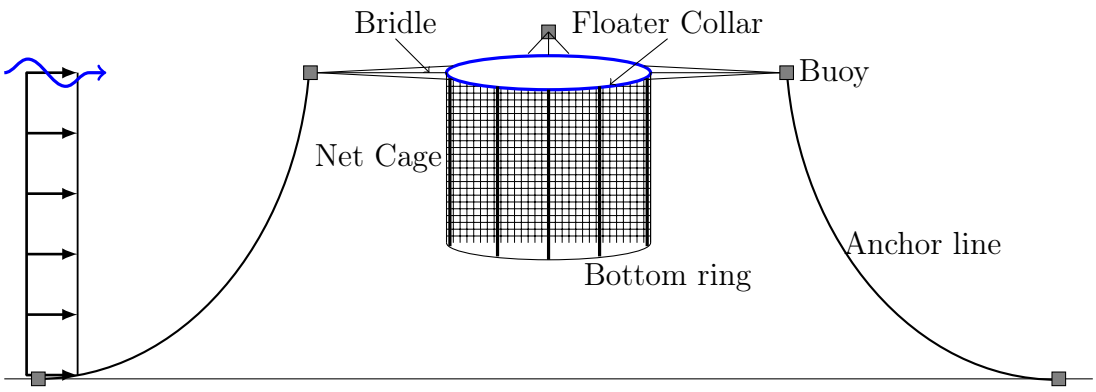


Figure 2.2: Schematic overview of the gravity net cage and mooring line system.

The gravity net cage is made up of: floater collar, net cage, bottom ring, chains and a mooring system. The components are all working together to maintain the cage's shape and position when exposed to environmental loads. The structure as a unit has to be considered as an interaction between all these compartments.

### Floating collar

The floating collar consists usually of two floatation rings. They are made of high density polyethylene (HDPE) and provide buoyancy to the structure. The floater serves also as a work platform for fish farmers for daily duties such as inspection and collection of dead fish.

### Net cage

The net cage surrounds the volume of water where the fish is grown, and is fastened beneath the floating collar. At present, most of the net cages are made of netting similar to that used for fish trawling. The net mesh is typically square or diamond shaped. Being made of a hydroelastic material makes it a deformable structure, and the net easily deforms by sea loads. To

make sure a satisfactory shape is maintained, the net cage is held down by weights.

### Bottom ring

The bottom ring provides weight to the net cage. It ensures that the geometric shape and volume are maintained when the net cage is exposed to waves and currents. Traditionally it has been tied to the floater by chains and connected to the net cage with ropes. This design has caused wear and tear between the chains and the net when the net is sufficiently deformed. An alternative design is to connect the gravity ring directly to the netting. This may lead to increased tension in the net cage.

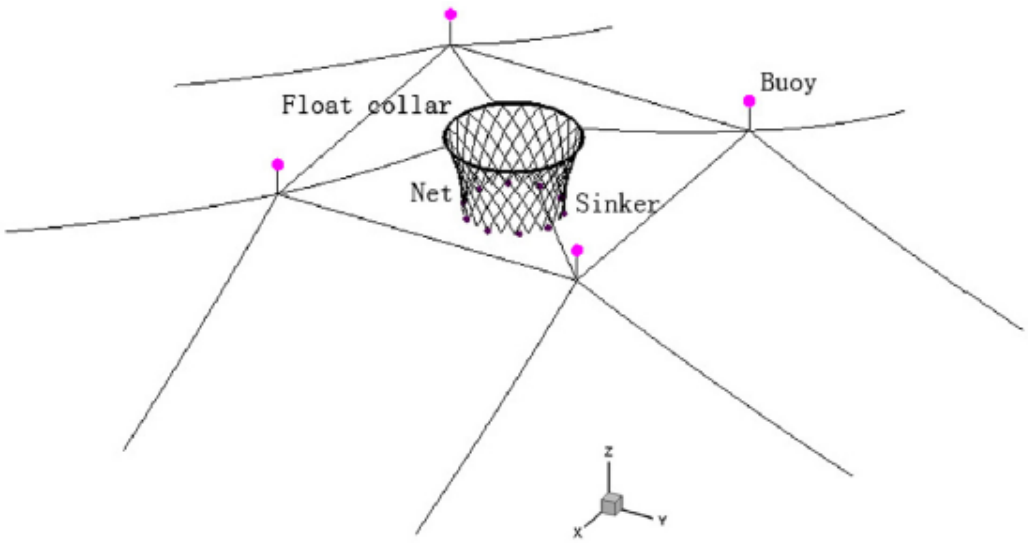


Figure 2.3: Overview of complete mooring system (Xu et al. 2013)

### Mooring system

The mooring system's main function is to keep the structure at a specific location. It also keeps the configuration of the elastic floater collars circular and carries the global forces. The mooring system is made up of several ropes, and the configuration is illustrated in figure 2.3. The different ropes

making up the mooring line system is denoted as in figure 2.2. The bridles are ropes which are equally distributed around the floater, and connect the floater collar to the surrounding squared shaped mooring frame. The buoys are placed in the corners of the mooring frame, and ensures buoyancy to the mooring line system. The anchor lines connect the frame corners to the seabed.

## 2.2 Environmental loads

The gravity net cage is generally exposed to wind, waves and currents. The loads acting on the structure will be the result of a fluid-structure interaction between moving sea water and the structure's movement, including deformations. Characterized by the hydroelastic behaviour, the gravity net cage is a complex structure to describe in terms of hydrodynamic loads.

### 2.2.1 Global loads

The mooring system carries the forces acting on the aquaculture structure and must be dimensioned according to the global loads, which mainly are due to horizontal forces on the floater and net cage (Kristiansen & Faltinsen 2012*b*). The particular contribution from floater collar and net cage will be outlined.

#### Hydrodynamic forces on the floater collar

Hydrodynamic loads on the floater are both current and wave induced. Located in the water surface, the floater collar is often modelled as a semi-submersed horizontal cylinder. Because the tube diameter is relatively small compared to the dimensioning wave length, it can be considered as a small-volume structure. In long waves, the floater nearly follows the waves.

Linear potential flow theory is assumed in the calculations of wave excitation forces, added mass loads and damping forces (Kristiansen & Faltinsen 2012*b*).

Floater collar response in surge and heave is observed to oscillate with the same frequency as incoming waves (Zhao et al. 2012). Numerical simulations

show that mean and total forces on the floater collar increase with longer wave period and larger wave height (Lader & Fredheim 2006).

#### Hydrodynamic forces and response of the net cage

The net experiences a water flow from the current and wave water velocity, leading to a net pressure drop and formation of a wake across the net panel (Klebert et al. 2013). Lift and drag forces are exerted on the panel, while viscous drag force is the dominating force (Kristiansen 2008). A more detailed explanation of loads on nets from currents are described in section 3.3.5.

## 2.3 Design aspects and mooring line load

For operational aspects, the sea based industry is concerned about mooring line tension, volume reduction of the cage system and floater collar motions.

### 2.3.1 Fish farm failure

Failure of a fish farm may lead to economical losses due to down time of the aquaculture plant and fish escape. Reasons for system failure and fish escape caused by severe environmental conditions are:

- Mooring system failure
- Rupture and tearing of net
- Snap loads

Critical structural parts are generally seen in the connections between the structural parts. However, the most fatal scenario is breakage of one mooring line, which leads to loss of the fish farm. This scenario can occur if the cage system encounters severe environmental forces, which may arise during a storm. In order to prevent this, a proper mooring system has to be designed.

### 2.3.2 Requirements for design

Large scale fish escapes have been reported due to mooring failure or rupture of the net between the floater and the net cage. To cope with the problem, technical regulations for design and investments in research were established in Norway the last decades (Jensen et al. 2006).

#### Norwegian technical standard

The Norwegian technical standard (NS 9415) was implemented through Norwegian legislation on April $1^{st}$ 2004 and revised in 2009. NS 9415 describes the requirements for site survey, risk analysis, design and dimensioning of fish farms (Jensen et al. 2006). Special accredited, independent companies assess the fish farms.

The introduction of NS 9415 lead to a dramatic reduction in fish escape (Jensen et al. 2006). Partly, due to an increased attention to regularly maintenance and requirements for replacement of old equipment. Additionally, an increased focus and research on the structural parts of fish farms were seen.

The requirement for accidental loads are summarized here, referring to (Standard 2009) for further details.

#### Requirement for site classification

A location proposed for fish farming must be investigated regarding topography and environmental loads. The considered environmental loads are waves, currents, wind and ice. Waves and currents are outlined here.

Specific measurements or long time statistical analysis of currents are required at the fish farm location (Standard 2009). A minimum dimensioning value for current is 0.5 m/s (Jensen 2006). Dimensioning waves are based on diffraction calculations or site specific measurements.

#### Requirement for loads

General design and load requirements are given in section 6.0 in Standard (2009). The probable load situations during operation and maintenance of the fish farm must be accounted for.

The accidental loads are defined as:

1. Rupture of mooring line
2. Damage of floater

It is required to evaluate rupture load of the mooring line carrying the largest load as well as rupture in the mooring line most critical for the whole fish farm's strength. Also, rupture in connections of mooring lines must be evaluated (Standard 2009).

The floaters' functionality must be evaluated, including its behaviour when punctuated and water intake. The design must also be evaluated in the case of loss of a floater. The floater has to be designed according to a 3-hour storm.

#### Load combinations

Load cases are assessed according to the design wave, design current and design wind. The largest of the two load combination of current and waves as presented in table 2.1 is considered the dimensioning load case.

Table 2.1: Combinations of environmental conditions (NS9415)

| Combinations | Current [year] | Wave [year] | Wind [year] |
|---|---|---|---|
| 1 | 50 | 10 | 10 |
| 2 | 10 | 50 | 50 |

### 2.3.3 Mooring line analysis

For a complete structural analysis of a floating fish farm, accurate assessment of the hydrodynamic forces on the floater and net cage is required. Numeri-

cal codes developed during the last decades aim to capture these features. A number of questions are still open to what factors are important when modelling the gravity net cage (Kristiansen & Faltinsen 2014). Earlier studies have shown that current constitutes a large portion of the total mooring line load (Huang et al. 2008).

The focus in this thesis is on mooring line force, representing the global loads acting on the system. The gravity net cage is analysed in a combination of currents and waves, and relative importance of current and wave force is studied. The applied environmental conditions can be considered as a combination of large currents and waves.

# Chapter 3

# Modelling the gravity net cage

In order to determine the gravity net cage's response and total forces numerically a mathematical model capturing the system's physical properties is required. The last couple of years, several numerical models describing the gravity net cage have been developed.

## 3.1 Steps in the analysis

Considering the gravity net cage in the water environment, one can identify the external forces acting on it as: hydrodynamic forces, gravitational forces, buoyancy forces and tension forces. All these forces have to be modelled accurately on the different compartments in order to predict the global forces and the dynamic behaviour of the system. The mathematical model also have to account for the material properties of the structural parts. The analysis is performed in the time domain and the forces, displacements and velocities are updated in each time step.

The main steps in the numerical program are:

1. Establish a model for the structural parts. This is to take into account the specific physical properties of the structure.
2. Determine all the forces acting on the structure. Establish a model for the external hydrodynamic forces.

3. Apply Newton's second law on the nodes, and solve the integrated system in the time domain. Forces, displacements and velocities are updated for each time step.

There is a strong coupling between the motion of the floater and the net, and the motions of the floater impact the net cage motions. The whole system of floater and net are solved for simultaneously in the numerical programs applied in this thesis. In the following, a description of the theory that forms the basis for the structural and hydrodynamic model of the floater collar and net cage is presented.

## 3.2 The floater

The floater is a circular plastic collar made of elastic high-density polyethylene (HDPE) pipes (Li & Faltinsen 2012). The floater may consist of one to three pipe circles, called tori. In calm water, it is assumed semi submerged. When exposed to waves, the floater motions will follow the waves due to its elastic properties (Faltinsen 2011).

Typical Young's modulus of elasticity for a HDPE type plastic is $E = 1000$ MPa, a yield stress $\sigma = 25$ MPa and a density $\rho = 60kg/m^3$ (Endresen 2011). The floater collar of the gravity net cage tested in Nygaard (2013) was made up if two concentric tori, and is illustrated in figure 3.1. The structural model and load model of the floater collar is presented.


Figure 3.1: Model of a fish farm floater collar consisting of two torus (Nygaard 2013)

### 3.2.1 Structural model

In order to determine the floater collar's motions, floater equations have to be established and solved. Li & Faltinsen (2012) developed a 3D-beam theory which is implemented in both numerical codes used in the simulations in this thesis.

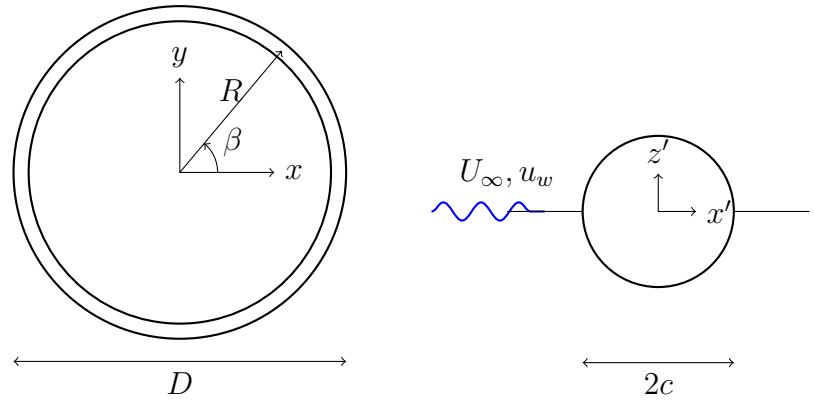


(a) Bird's view of a circular floater

(b) Sideview and cross section of a torus

Figure 3.2: Floater collar. Adapted from (Faltinsen 2011)

An overview of the torus configuration is given in figure 3.2a. The radial and vertical structural response is assumed to obey the Euler beam equation (Endresen 2011):

$$\begin{aligned} m\frac{\partial^2 v}{dt^2} + EI(\frac{\partial^4 v}{ds^4} + \frac{1}{R^2}\frac{\partial^2 v}{ds^2}) &= f_r(s,t) \\ m\frac{\partial^2 z_f}{dt^2} + EI\frac{\partial^4 z_f}{ds^4} &= f_z(s,t) \end{aligned} \tag{3.1}$$

where

| | |
|---|---|
| $v$ | is the radial response |
| $z$ | is the vertical response |
| $m$ | is the floater mass per unit length |
| $EI$ | is the structural bending stiffness |
| $f_z$ | is the vertical forces per unit length of the floater |
| $f_r$ | is the radial forces per unit length of the floater |

The motions of the torus is assumed to be described by perturbations around a circular shape, which is represented by sinusoidal modes in both horizontal and vertical direction (Kristiansen & Faltinsen 2012*b*). The motion of each point on the floater $(x_f, y_f, z_f)$ is described in 3.2. Structural damping from wave radiation is not considered (Li & Faltinsen 2012).

$$\begin{aligned} x_f(\beta,t) &= b_1 + v(\beta,t)\cos\beta \\ y_f(\beta,t) &= v(\beta,t)\sin\beta \\ z_f(\beta,t) &= \sum_{n=0}^{\infty} a_n(t)\cos(n\beta) \\ v(\beta,t) &= \sum_{n=2}^{\infty} b_n(t)\cos(n\beta) \end{aligned} \tag{3.2}$$

where

$a_0$ represents heave
$a_1$ represents pitch
$a_2$ represents the first vertical elastic mode
$b_1$ represents surge
$b_2$ represents the first horizontal elastic mode (ovalization)
$\beta$ is the angle in the xy-plane of the torus, see figure 3.2a

### 3.2.2 Hydrodynamic force

In long waves, the elastic floater will nearly follow the waves. For the wave excitation and added mass loads on the floater, potential flow theory is considered (Kristiansen & Faltinsen 2012*b*). Long wave theory is assumed for the incident waves, and the waves propagate along x-axis. Both three-dimensional flow and frequency effects are essential for the considered vertical wave loads and responses (Li & Faltinsen 2012).

The total external forces acting on the floater, $f_r$ and $f_z$, can be expressed as:

$$f_{r,z} = f_{r,z}^{FK} + f_{r,z}^{diff} + f_{r,z}^{a} + f_{r,z}^{drag} + f_{r,z}^{nc} + f_{r,z}^{m} \tag{3.3}$$

where

$f_{r,z}^{FK}$ is the Froude Kriloff force
$f_{r,z}^{diff}$ is the diffraction force
$f_{r,z}^{a}$ is the added mass force
$f_{drag}$ is the drag force
$f_{r,z}^{nc}$ is the net cage forces transferred via ropes and cables
$f_m$ is the mooring force transferred via ropes and cables

## 3.3 The net cage

A net cage is formed by several million twines, and each unit can be considered as a cylinder with length $l_w$ and diameter $d_w$ as illustrated in figure 3.3.

The twines are usually oriented in a square or square-diamond pattern.

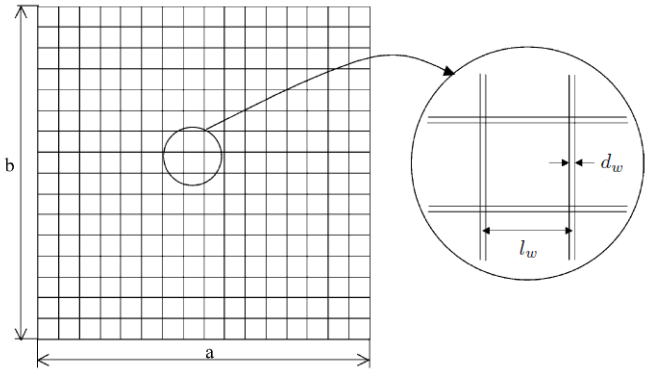


Figure 3.3: Net mesh geometry (Tsukrov et al. 2003)

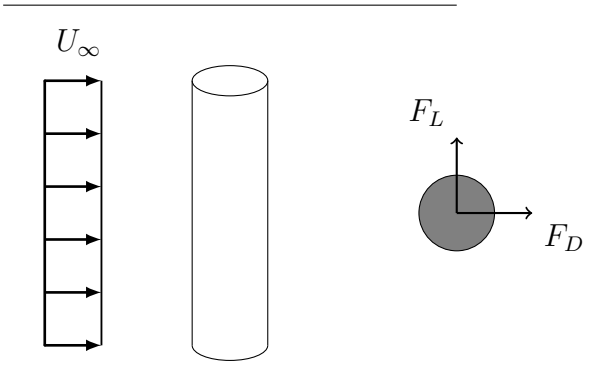


Figure 3.4: Drag and lift force on a submerged cylinder

### 3.3.1 Force on a submerged cylinder

According to Blevins (2003), the viscous force and flow separation force on a submerged, slender cylinder in current can be decomposed into two parts: One in-line with the flow direction and the other perpendicular to the cylinder as illustrated in figure 3.4. The forces are calculated from equation (3.4) and (3.5).

$$F_D = \frac{1}{2}\rho A C_D U_\infty^2 \tag{3.4}$$

$$F_L = \frac{1}{2}\rho A C_L U_\infty^2 \tag{3.5}$$

where $\rho$ is the density of the water, A is the projected area, $C_D$ and $C_L$ are drag- and lift coefficient and $U_\infty$ is the ambient current velocity.

In currents and waves, the drag an lift is assumed to follow equation (3.4) and (3.5), by replacing $U_\infty$ with the relative velocity. The instantaneous relative water flow at the twines is described by:

$$U_{rel} = rU_\infty + u_w - u_j \tag{3.6}$$

where $U_{rel}$ is the relative velocity between net panel and the water velocity, $U_\infty$ is the ambient current velocity, $u_w$ is the water particle velocity and $u_j$ the velocity of the net cage. r is the velocity reduction factor, which is 1 at the net cage front and reduced at the rear net cage wall according to e.g. equation (3.10). By considering wave flow as quasi-steady due to high KC-numbers, the force model is applicable for waves as well (Kristiansen & Faltinsen 2014). An illustration of the forces on a net panel is presented in figure 3.5.

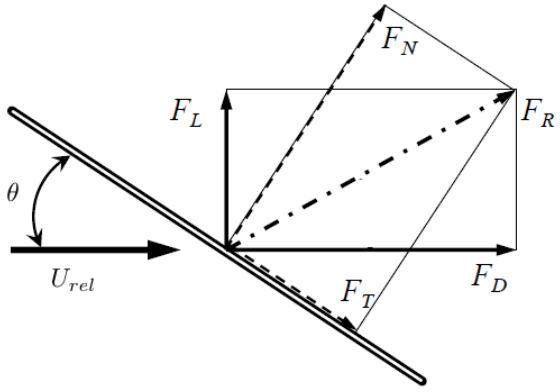


Figure 3.5: Drag and lift forces and angle of attack ($\theta$) (Enerhaug et al. 2012)

where $U_{rel}$ is the relative water flow at the twines, $\theta$ is the angle of attack, $F_D$ is the drag force, $F_L$ is the lift force, $F_N$ the normal force and $F_T$ the tangential force component.

### 3.3.2 Parameters describing the net panel

The main parameters describing a net cage, which also are relevant when calculating the drag and lift coefficients for a net panel are:

- Solidity ratio of the net, Sn
- Reynolds number at the twines, Rn
- Angle of attack between the twine and incoming water flow, $\theta$

The solidity ratio describes the fraction of projected area of the twines to the total net area. For a square-woven net:

$$Sn = 2 \cdot \frac{d_w}{l_w} - \left(\frac{d_w}{l_w}\right)^2 \tag{3.7}$$

where $d_w$ is twine diameter and $l_w$ is twine length.

The solidity ratio of a fish net is adjusted to the production purposes; a net cage used for aquaculture typically has a solidity ratio between 0.20-0.35. A net cage for young fish requires finer mesh than a net cages for mature fish. Another aspect impacting solidity ratio is bio-fouling. When located in the ocean, biological growth on the mesh leads to increased twine diameter and decreased bar length, and is often modelled numerically as increased twine diameter. In this thesis, a net with solidity ratio of 0.26 is studied.

Reynolds number is a parameter related to the flow characteristic around each twine:

$$Rn = \frac{U_{rel} d_w}{\nu} \tag{3.8}$$

where $U_{rel}$ is the relative water velocity, $d_w$ is twine diameter and $\nu$ the kinematic viscosity of the water.

The twines will be orientated in an arbitrary angle between 0° and 90°, relative to the incoming water flow. This is denoted the angle of attack, $\theta$, which is illustrated in figure 3.5. The angle of attack influences the drag force on a twine, and a small angle of attack induces almost zero drag force

while an angle of 90° induces the largest drag force (Kristiansen & Faltinsen 2012*a*).

### 3.3.3 Flow through net panels

When considering the flow across a net, it will be subject to a pressure drop proportional to the velocity squared (Klebert et al. 2013), and consequently the panel will experience a drag force and a reduced flow velocity. The description of water flow velocity across the net panel is of importance to predict the forces precisely. The adjusted water flow at the twines, the reduced velocity at the rear wall of a net cage and the wake effects behind a net panel are described in the following.

#### Adjusted water flow velocity

When passing the net, the water velocity will speed up due to mass conservation. To obtain correct Reynolds number at the twine, the water flow velocity must be computed accurately. The characteristic cross flow velocity at the twines can be described as (Kristiansen & Faltinsen 2012*a*):

$$U_S = \frac{U_{rel}\cos\theta}{1 - Sn},\ 0 \leq \theta \leq \pi/_4 \tag{3.9}$$

where $U_{rel}\cos\theta$ is the far field cross-flow velocity and $(1 - Sn)^{-1}$ is the factor accounting for the local speed up.

By applying the the adjusted water flow velocity at the twines, a more accurate Reynolds number is found.

#### Reduced velocity

Due to the velocity loss across a net panel, the incoming current velocity on the back wall of a net cage will be reduced. Løland (1993) proposed a velocity reduction factor r for downstream flow velocity relative to the upstream velocity, presented in 3.10.

$$u_{wake} = rU_{\infty}$$
$$r = 1 - 0.46C_D \tag{3.10}$$

**Wake effects**

Løland (1991) analysed the wake generated behind a panel. The panel was approximated by cylinders in the horizontal and vertical direction. He estimated the wake to be a sum of the individual 2-D wakes behind each cylinder, and obtained an expression of flow distribution downstream a net panel.

**Net cage deformation**

Current loads on net cage arrays lead to a deformation and reduction in available net cage volume. Increased current speed induces increased loads and excess deformation. Tank experiments and full scale experiments have showed this Klebert et al. (2013). However, there are some benefits from high current velocity which is increased fresh water flow to the net cage and efficient waste and excrement transportation.

The deformation for large current velocities $(0.5 - 1.0)$m/s can be excess. Moe et al. (2010) reports 70% volume reduction at current velocity of 0.5 m/s. It is of importance to limit the deformations, due to the fish's welfare.

### 3.3.4 Structural model

The structural properties of the net has to be modelled. The net cage is discretized into elements which can be modelled as net panels, trusses, bars, catenary lines or other structural models (Moe et al. 2010). All models represents the twines structural features. In some models a net panel represents the physical twines. In other models the net panels are modelled as bars or trusses which capture the features of many twines.

### 3.3.5 Hydrodynamic load model

Figure 3.5 shows the lift and drag force components acting on a twine. In the literature there exists mainly two approaches to model the drag forces on a net panel.

**I. Morison based**: By summing drag force from each twine

**II. Screen model**: By summing drag force from every net panel

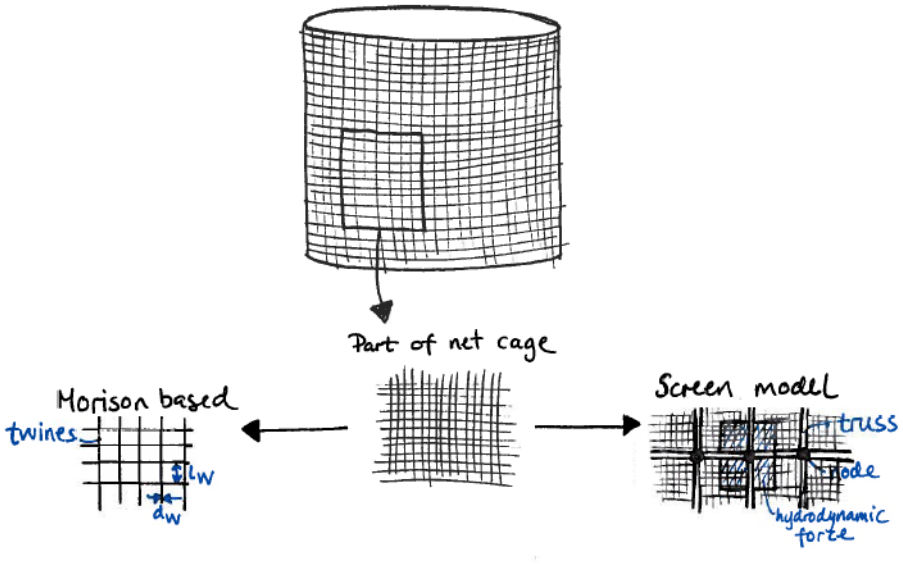


Figure 3.6: Hydrodynamic load model, approach I (left) and II (right)

The approaches distinguish in the way they compute the viscous loads on a net panel as illustrated in figure 3.6. While type I determines the drag coefficient based on the twine diameter and Reynolds number, type II computes the drag coefficient based on the area's solidity ratio, angle of attack as well as the local Reynolds numberat the twines.

### Approach I - Morison based

In approach I, the total drag on a net panel is obtained by summing drag and lift forces on the individual knots and twines (Lader & Fredheim 2006). The drag force coefficient is determined from Reynolds number at the twine, as seen in equation (3.11). In this method the interaction between two neighbouring twines are usually not accounted for. This type of load model is implemented in FhSim, described in chapter 4.1.

$$\begin{aligned} F_D &= \frac{1}{2}\rho A C_D(Rn)|U_{rel}|U_{rel} \\ F_L &= \frac{1}{2}\rho A C_L(Rn)|U_{rel}|U_{rel} \end{aligned} \tag{3.11}$$

### Approach II - Screen model

In approach II, the net cage is divided into net panels. The force coefficients are determined based on the area's solidity ratio (Sn), angle of attack ($\theta$) and the Reynolds number (Rn) at the twines, as presented in equation (3.12).

Løland (1991) and Kristiansen & Faltinsen (2012*a*) have developed this type of hydrodynamic force models. The models are reviewed.

$$\begin{aligned} F_D &= \frac{1}{2}\rho A C_D(Sn, Rn, \theta)|U_{rel}|U_{rel} \\ F_L &= \frac{1}{2}\rho A C_L(Sn, Rn, \theta)|U_{rel}|U_{rel} \end{aligned} \tag{3.12}$$

### Løland's formulas

From curve fitting of experimental data by Rudi et al (1988), Løland presented a model for viscous loads on flat panels by the two formulas in equation (3.13).

$$C_D(Sn,\theta) = 0.04 + (-0.04 + 0.33Sn + 6.54Sn^2 - 4.88Sn^3)cos\theta$$
$$C_L(Sn,\theta) = (-0.05Sn + 2.3Sn^2 - 1.76Sn^3)sin2\theta \tag{3.13}$$

The formulas are valid for a solidity ratio in the range $0.13 - 0.317$ and angle of attack in the range $0° - 90°$.

### Kristiansen and Faltinsen's screen model

The aim of their work was to improve the drag and lift coefficients from Løland (1991)'s formulas (3.13) for a screen type force model. The generalization was suggested to include Reynolds number dependency, account for a wider range of solidity ratios, as well as include an improved dependency of angle of attack. To include these properties, the expression of $C_D$ and $C_L$ had to be more precise. The adjusted water flow velocity was taken into account. The theories by Kristiansen & Faltinsen ($2012a$) are based on earlier experimental data and a new combination of the experimental expressions. The detailed expressions for drag and lift coefficients specified for small angles of attack $\theta < \frac{\pi}{4}$ and large angles of attack, $\theta > \frac{\pi}{4}$ are given in appendix A.1.

The load model was shown to be valid for a broader range of current velocity and angle of attack, than previous experimental equations (Kristiansen & Faltinsen $2012a$). This method is implemented in fishFarm.

The presented Morison load model is implemented in the later applied numerical software FhSim, while the screen type load model is implemented in the later utilized numerical solver, fishFarm.

# Chapter 4

# Software

To simulate the gravity net cage and determine global forces, two of the available software programs are used in this thesis. FhSim is SINTEF Fisheries and Aquaculture inhouse software. The code developed by Kristiansen & Faltinsen (2012*a*) for current only, and further developed for combined waves and current by Kristiansen & Faltinsen (2014) is in this work denoted as "fishFarm". An overview and modelling principles of FhSim and fishFarm is outlined in the following sections.

## 4.1 FhSim

Development of FhSim started in 2006 and is still an ongoing project for SINTEF Fisheries and Aquaculture. FhSim serves as a common platform to simulate different marine systems in the time domain.

### 4.1.1 General

FhSim is object oriented, and is organized in a way so that a complex structure is built by several substructures. In addition to the specific model, there are support functions such as integrator, file input/output, external ports and visualization. An overview of the organization of FhSim is presented in figure 4.1.

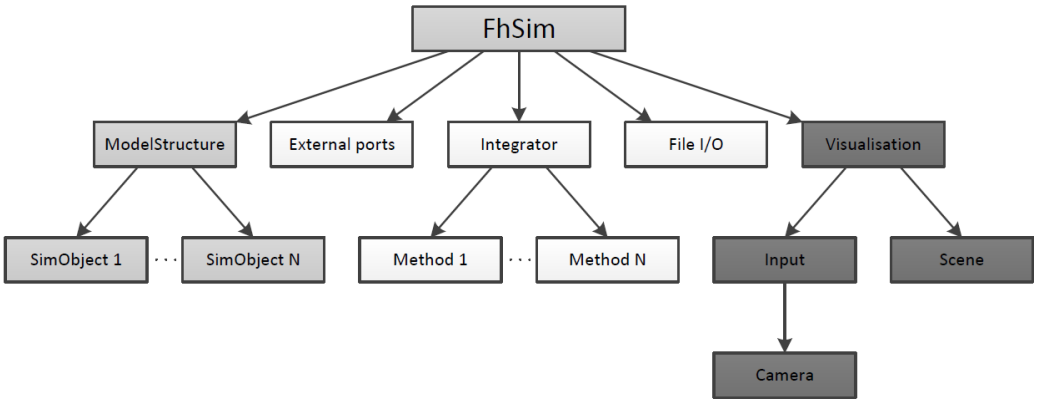


Figure 4.1: An overview of FhSim (Reite et al. 2014).

### 4.1.2 Realizing an aquaculture net cage model

The model of a gravity net cage is realized by a floater collar, net cage, chains, bottom ring and ropes making up the mooring system. A visualization can be seen in figure 4.2. The model is generated by an input file providing information about all sub objects, geometric and material properties and the environmental conditions. FhSim is able to simulate environmental conditions with current and regular or irregular waves.

The system is solved in the time domain by use of one of several available integrator methods such as Euler, Heun's or Runge Kutta method. The output is written to a csv. formatted file. A more detailed explanation of the the mathematical model of the floater and net cage is presented in the following sections.

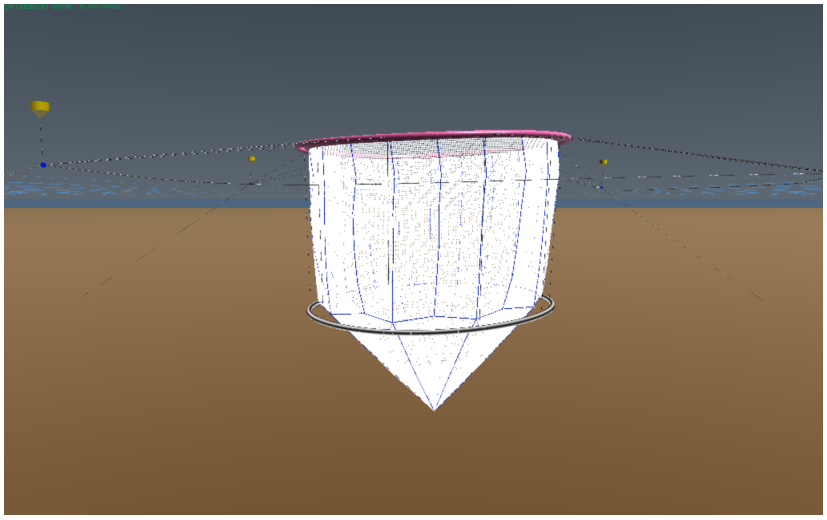

Figure 4.2: Visualisation of the simulated system A in FhSim

### 4.1.3 Floater

The structural theory implemented in FhSim is the 3D-beam theory as presented in section 3.2.1. The floater is modelled as a flexible continuous circular ring with six degrees of freedom. Since the tested floater collar consists of two rings, the implemented theory accounts for the difference between physical and numerical modelling.

### 4.1.4 Net cage

#### Structural model

The structural model in FhSim is based on Priour (1999)'s modelling of net structures. The net cage is discretized by triangular net elements equipped with nodes as shown in figure 4.3. It is assumed that the elongation and elasticity modulus are constant for each triangular element (Priour 1999). External forces acting on the net are distributed equally between the nodes and Newton's second law is solved for in each time step. The net is reinforced by ropes inserted in the net.

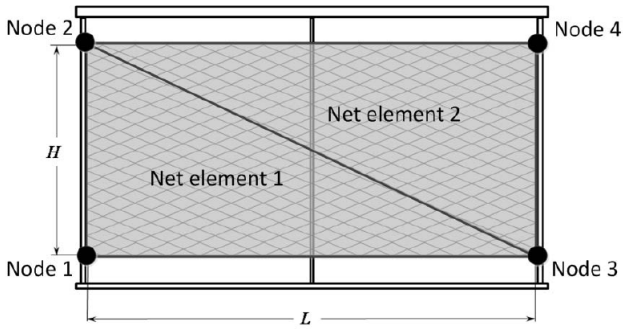


Figure 4.3: Priour's element (Enerhaug et al. 2012).

#### Hydrodynamic model

The hydrodynamic forces acting on the triangular element are found by applying Morison's equation on the twines, as described in section 3.3.5. The drag and lift forces are calculated for one random horizontal and one random vertical oriented twine, and the water flow velocity and twine configuration is assumed constant within one element. Total drag and lift is obtained by multiplying the drag force with the number of twines within one element. The total force is evenly distributed between the three corner nodes in the element (Enerhaug et al. 2012). The wake effect and adjusted water flow velocity is accounted for.

### 4.1.5 Simulation and validation

At present, FhSim contains mathematical models for all compartments of the gravity net cage. Earlier validation studies have shown satisfactory results for the net cage in small and intermediate net deformations (Endresen et al. 2014).

However, there are still lack of studies where a complete fish farm system including all subparts are simulated and validated. Endresen et al. (2014) performed such studies, but the results are not clearly confirming a realistic modelling of the integrated system.

## 4.2 fishFarm

The theory which is implemented in fishFarm is developed by Kristiansen & Faltinsen (2012*a*). The code is further developed to include currents and waves in Kristiansen & Faltinsen (2014). The numerical code applies an equivalent truss structural model and a screen type hydrodynamic force model.

### 4.2.1 General

fishFarm is a numerical code solving the net cage with an elastic floater in currents and waves. Currently, the code serves to model the gravity net cage with an elastic floater, bottomless net cage, discretized bottom weights and mooring lines. Although the model is not a complete gravity net cage system, it represent the system's main structural and environmental particulars (Kristiansen & Faltinsen 2012*b*).

In the numerical model, the motion of all compartments including the net cage, bottom weights, floater and moorings are solved for simultaneously. The hydrodynamic forces acting on the net and floater are calculated and a linear system of equations for the tensions in all the net cage and mooring trusses are solved for. The kinematic constraint, which requires that no twines are elongated, is the criterion to solve the system of equations for tensions. The systems is solved in each time step according to Newton's second law, and the node positions, velocities and tensions are updated.

### 4.2.2 Floater

The floater is modelled as described in section 3.2.1. In Kristiansen & Faltinsen (2014), the floater axial stiffness is included in the model.

### 4.2.3 Net cage model

#### Structural model

In FhSim, the implemented structural model is the equivalent truss element introduced by Marichal (2003). The net cage is discretized into net panels where one truss represents the structural features of the twines for this net panel area, as illustrated in figure 4.4. Thus a grid of trusses represents the net panels of a whole cage as shown in figure 4.4a. The interfaces between the trusses, become the nodes where the sum of forces are lumped into. Figure 4.4b shows an illustration of the net truss element. The external forces acting in the nodes are calculated from the four shaded adjacent areas.

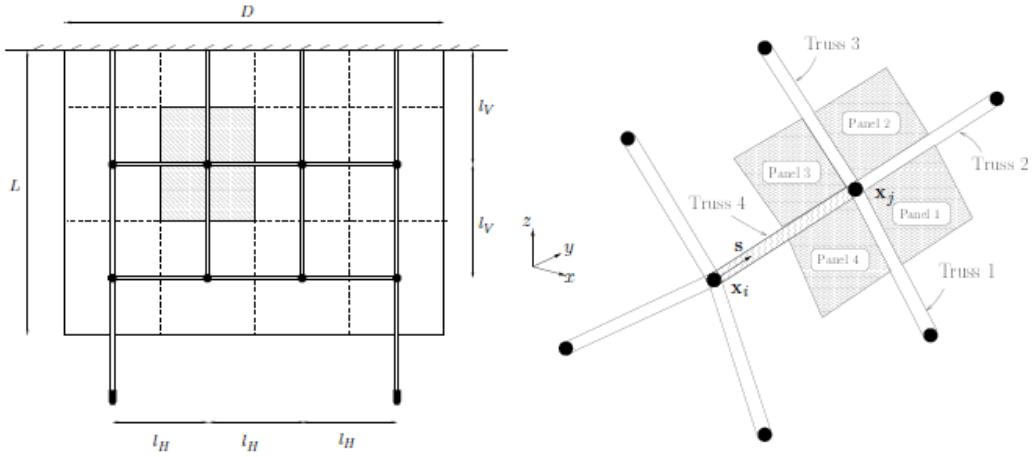


(a) (b)

Figure 4.4: Equivalent truss model of planar net, overview to the left and detail to the right (Kristiansen & Faltinsen 2012*a*)

#### Hydrodynamic force model

The viscous force is modelled by the screen type force model developed by Kristiansen & Faltinsen (2012*a*). The drag coefficient is determined for an area of the net cage as described in section 3.3.5. This have shown improvements of load prediction for large net deformations and high current velocities Kristiansen & Faltinsen (2012*a*).

### 4.2.4 Simulation and validation

The code was developed and validated for a net cage to experiments performed in the towing tank in the MC lab at NTNU (Kristiansen & Faltinsen 2012*b*). Kristiansen & Faltinsen (2014) presents a validation study for the net cage and the floater. The code shows satisfactory agreement for both current only and in a combined current and wave condition.

It is seen that FhSim and fishFarm have the similar implemented model for floater collar, while the hydrodynamic load model on the net cage is different. The results of a comparison study between the numerical codes is presented in chapter 7.2.

# Chapter 5

# Methodology

In this thesis the mooring line loads, which represent the global loads acting on the gravity net cage are studied. The loads are analysed from an experimental and numerical point of view, and the effects from currents and waves are investigated. The main focus is to examine the global mean loads in the experiments, and whether the simulation tools are able to capture the load's features.

As an approach to critical loads, an attempt to investigate the mean loads in a combination of large current and waves is made. The selected sea states and current conditions can be considered extreme for this type of structure.

## 5.1 Objective of the analysis

The thesis consists of two main objectives:

1. From the available experimental results from Nygaard (2013), the purpose is to investigate the fish farm's mooring load features in different combinations of irregular waves and current.
2. Perform a comparison study of the numerical software FhSim. The validation work includes both a comparison to the experimental results mentioned above, and a comparison to a second available numerical program fishFarm.

## 5.2 Steps in the analysis

Two models of the gravity net cage are subject for the analysis in this thesis. These two systems are denoted system A and system B, and are presented in figure 5.3 and 5.4 in section 5.3. The reason for using two systems is that the systems have different advantages and limitations in terms of available experimental data, model complexity and applications of the numerical programs. A more detailed description of the systems is given in section 5.3

The work is performed in these steps:

1. Investigate the features of the mooring line loads', by examining recent experiments of system A in the ocean basin. The results have been made available by SINTEF Fisheries and Aquaculture. A net cage design with complete mooring system is tested in regular and irregular waves+current

2. Simulate a model of system A in FhSim, and compare the results to the experimental results presented in 1.

3. Simulate a model of system B in FhSim and fishFarm, which is the similar setup as studied in Kristiansen & Faltinsen (2012*b*) and compare the programs load estimation. Perform a validation study of FhSim in terms of global mean load computation by comparing to the predicted results and existing experimental results presented in Kristiansen & Faltinsen (2012*b*).

The float digram in figure 5.1 gives an overview of the performed analysis.

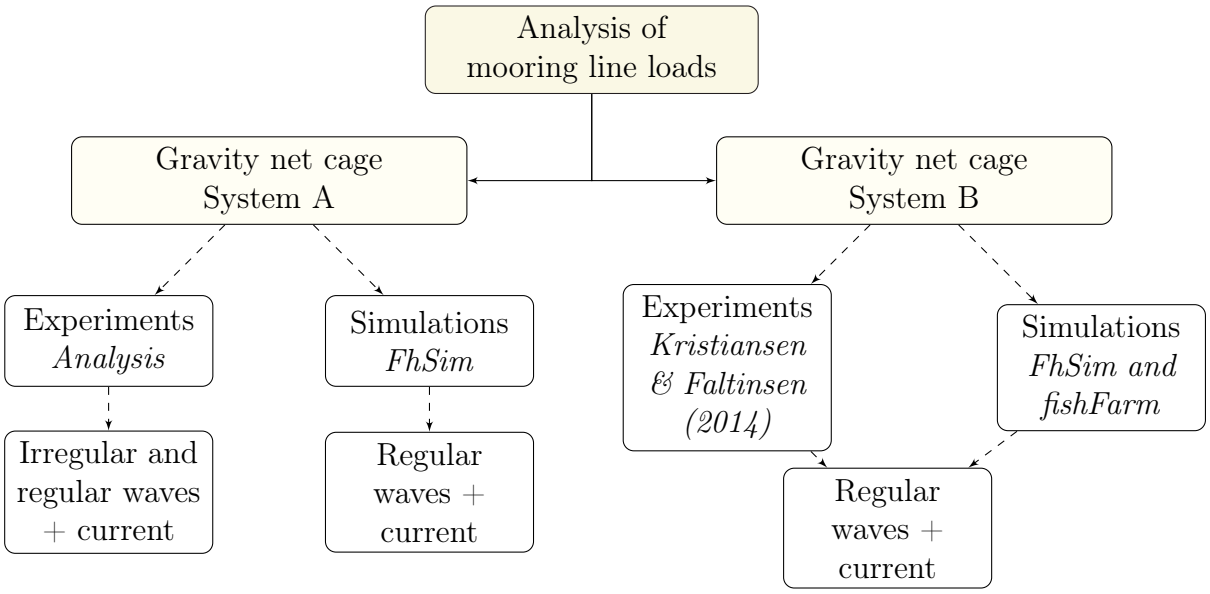


Figure 5.1: Float chart of the methodology.

## 5.3 Description of the models

Two different experimental set-ups of the gravity net cage are described, denoted system A and system B. The only similarity is that they both are models of a gravity net cage structure with a solidity ratio of 0.26. The two systems are different in terms of dimensions, bottom ring modelling, mooring line set-up and whether chains are present. System A is used as a mean for investigating mean loads features in irregular waves and current. The regular waves and current conditions forms the basis for the comparison study to FhSim simulations. System B is designed to be modelled and simulated in both utilized software.

### 5.3.1 System A

Experiments of a gravity net cage with a complete mooring system were executed in the ocean basin laboratory at MARINTEK in May 2013 (Nygaard

2013). The main purpose was to investigate the interaction between the different compartments in large currents and waves, and determine the capacity of the design. Model scale of 1 : 16 was utilized to include all physical effects.

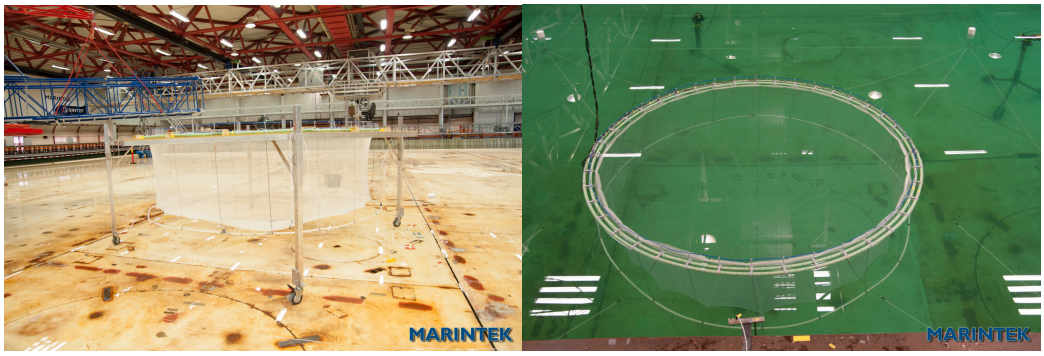


(a) Model in air (b) Model in water

Figure 5.2: Model of system A installed in the ocean basin. MARINTEK, Tyholt. Photo: Nygaard (2013)

The model is a gravity net cage with mooring line system, a floater, bottom ring, net cage and chains as seen in figure 5.2. Dimensions are presented in table 5.1. The full scale diameter is 50m and the depth of the cylindrical part is 15m. The floater is made up of two concentric rings. The mooring line system is presented in figure 5.3 and consists of bridles, mooring frame, buoys and anchor lines connected to the seabed. The dots in figure 5.3 indicate the locations of force sensors. Red dots indicate anchor line force, blue points indicate buoy chain force and black dots indicate where bridle force is measured.

The primary purpose of the conducted experiment was visual inspection of the interactions between the comprising structural compartments. The tested environmental conditions are rather limited of what is necessary for a complete validation study. A set of six environmental conditions was executed for regular waves and currents. For irregular waves, six selected sea states were run for the current velocities U=0.5m/s and U=0.7m/s. Floater collar motions were not measured. The wave probes were located to the side of and in front of the net cage. For further descriptions it is referred to (Nygaard 2013).

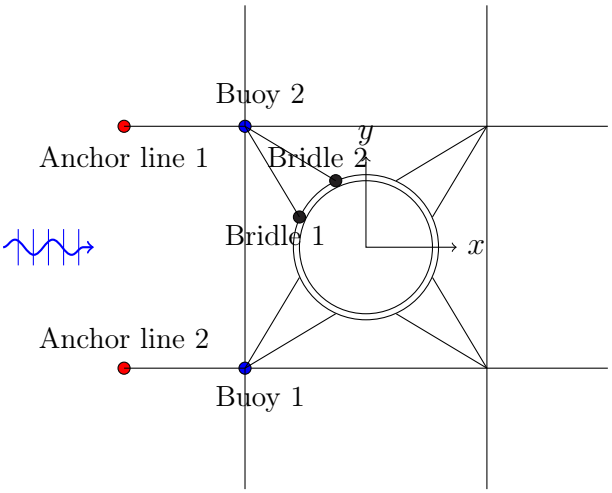


(a) Bird's view

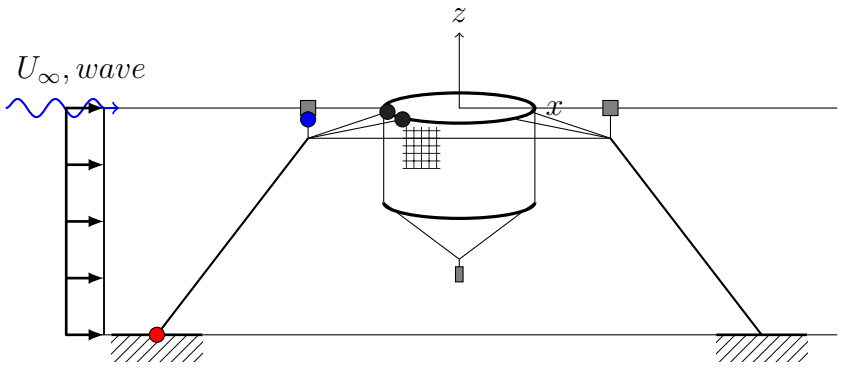


(b) Sideview

Figure 5.3: Mooring line system.

Table 5.1: Parameters for test setup A

| Description | Parameter | Unit | Model scale | Full scale |
|---|---|---|---|---|
| *Floater:* | | | | |
| Inner diameter | $D_f$ | m | 3.125 | 50 |
| Pipe diameter | $D_p$ | mm | 28.1 | 450 |
| Pipe wall thickness | $t_p$ | mm | 1.60 | 25.6 |
| Module of elasticity | E | MPa | 62.5 | 1000 |
| Moment of inertia | EI | $Nm^2$ | 0.74 | 771 500 |
| *Net cage:* | | | | |
| Diameter | $D_{net}$ | m | 3.125 | 50 |
| Depth, cylindrical part | $H_{cyl}$ | m | 0.938 | 15 |
| Depth, conic part | $H_{con}$ | m | 0.625 | 10 |
| Solidity | Sn | | 0.26 | 0.26 |
| *Bottom ring:* | | | | |
| Diameter | $D_f$ | m | 3.125 | 50 |
| Pipe diameter | $D_p$ | mm | 17.5 | 280 |
| Pipe wall thickness | t | mm | 25.5 | |
| Module of elasticity | E | MPa | 1000 | 1200 |
| Weight | $w_s$ | kg/m | 0.1953 | 50 |

### 5.3.2 System B

Experiments of a net cage model with scaling ratio 1 : 25 were executed in the MC-lab at NTNU, Trondheim 2011. The main purpose was to obtain experimental results to validate the numerical code fishFarm, but also to study the system physically (Kristiansen & Faltinsen 2012*b*).

The model is a gravity net cage with a single tubular floater and a net cage with some simplifications. The setup is designed for a towing test, and the bridles are attached to the carriage. The bottom ring is modelled with discretized weights, the bottom is not present and there are no chains present. The gravity net cage is fastened to the carriage with bridles. Note that the stiffness differs between the side and the front and aft mooring lines. The side mooring lines are stiff in order to prevent ovalization of the floater in large currents, while the front and aft mooring line are installed with springs

Kristiansen & Faltinsen (2012*b*). The experimental set-up is illustrated in in figure 5.4 and the dimensions of the components are listed in table 5.2.

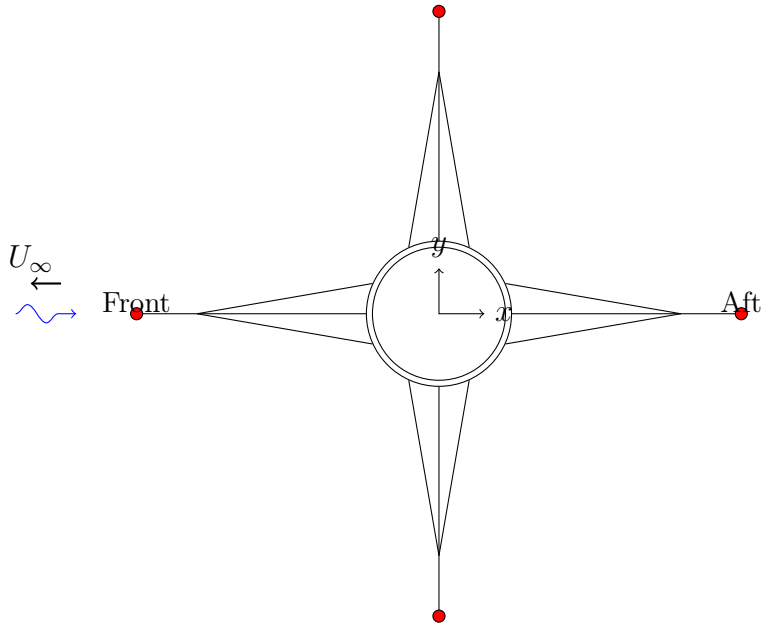


(a) Bird's view

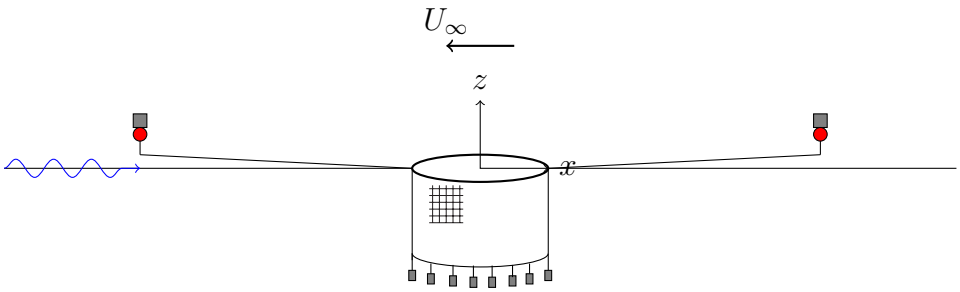


(b) Sideview

Figure 5.4: Model of system B installed in the towing tank. Adapted from: Kristiansen & Faltinsen (2012*b*)

Table 5.2: Parameters for the net cage system B

| Description | Parameter | Unit | Model scale | Full scale |
|---|---|---|---|---|
| *Floater:* | | | | |
| Outer diameter | $D$ | m | 1.5 | 37.5 |
| Pipe diameter | $D_p$ | mm | 30 | 0.75 |
| Module of elasticity | E | MPa | 300 | |
| Floater bending stiffness | EI | $Nm^2$ | 0.136 | |
| Mass per meter | $m_f$ | kg/m | 0.127 | |
| Floater density | $\rho_f$ | $kg/m^3$ | 960 | |
| *Net cage:* | | | | |
| Diameter | $D_{net}$ | m | 1.5 | 37.5 |
| Depth | $L$ | m | 1.3 | 32.5 |
| Twine diameter | $d_t$ | mm | 0.8 | |
| Solidity | Sn | | 0.26 | 0.26 |
| Module of elasticity | E | Pa | $1{\cdot}10^{12}$ | |
| *Bottom weights:* | | | | |
| Number | n | | 16 | |
| Mass in air | $M_{bw}$ | | 16x75g | |
| *Mooring lines:* | | | | |
| Spring stiffness | $k_s$ | N/m | 44 | $27.5\text{x}10^3$ |

## 5.4 Post processing

Time series of force measurements from experiments and simulations are post processed and Froude scaled according to scaling factors presented in appendix B. It is ensured that the mean force is computed from the steady state part of the time series. All presented results are in full scale dimensions.

# Chapter 6

# Experimental results

Results from the conducted experiment of a gravity net cage with complete mooring line system (system A) are analysed. The focus is on mean loads in the mooring lines. This chapter is divided into results from regular wave tests and irregular wave tests.

The tested conditions are a set of regular or irregular waves in combination with current velocities U=0.5m/s and U=0.7m/s. These current conditions are considered large for the conventional gravity net cage.

## 6.1 Regular waves and current

### 6.1.1 Total mean force

Table 6.2 presents the calculated mean force in bridles, buoy chains and anchor lines of the front mooring lines. Pretension is subtracted and the mean load describes the environmental impact on the system. The average of mean force in bridles, buoy chains and anchor line is presented. For wave and current parameters, see table 6.1.

Table 6.1: Test matrix for system A

| Case name | U [m/s] | H [m] | T [s] |
|---|---|---|---|
| C1 | 0.5 | - | - |
| C2 | 0.7 | - | - |
| W1 | - | 2.5 | 6.0 |
| W2 | - | 2.5 | 8.0 |
| CW1 | 0.5 | 2.5 | 6.0 |
| CW2 | 0.5 | 2.5 | 8.0 |

Table 6.2: Mean force in mooring system [kN].

| | Bridle 1 | Bridle 2 | Average | Buoy chain | Anchor line |
|---|---|---|---|---|---|
| C1 | 13.4 | 32.8 | 23.1 | 8.3 | 23.0 |
| C2 | 29.6 | 50.7 | 40.1 | 17.0 | 47.3 |
| W1 | 2.1 | 13.0 | 7.5 | 2.8 | 8.0 |
| W2 | 0.2 | 4.3 | 2.3 | 1.3 | 3.5 |
| CW1 | 21.6 | 43.6 | 32.6 | 15.5 | 38.1 |
| CW2 | 19.0 | 38.4 | 28.7 | 12.3 | 32.4 |

By comparing the magnitude of the mean force throughout the mooring system in table 6.2, it is seen that the largest mean loads occurs in bridle 2 and in the anchor line for all tested conditions. The obtained mean forces are used in the validation study of FhSim in chapter 7. Total mean force from currents is further used as a reference value in the combined waves and load conditions, and is presented as dashed lines in figure 6.1.

### 6.1.2 Estimation of drag coefficient

From the current only results (C1 and C2) it is possible to evaluate a drag coefficient for the mooring line load based on equation 3.4. In order to determine the projected area, the configuration of a net cage in calm water is considered. The solidity ratio is accounted for. The projected area is assumed to be the the sum of the front and aft net wall area. The drag coefficients are presented in table 6.3, and are later utilized in the computation of estimated mean dynamic load in section 6.2.2.

Table 6.3: Drag coefficient for one anchor line.

| | U [m/s] | $C_D^0$ [-] |
|---|---|---|
| C1 | 0.5 | 0.345 |
| C2 | 0.7 | 0.366 |
| Average | | 0.35 |

From table 6.3, it is seen that a fairly similar drag coefficient is predicted from the measured mean load for both current velocities. This indicates that the measured mean force coheres with the theoretical ratio between the total drag force for the two considered current velocities. However, it is just an indication. In the further analysis, the mean load in the anchor line is studied.

## 6.2 Irregular waves and current

The results are based on the irregular runs of 6 sea states, as listed in table 6.4. All runs are executed for two current velocities, U=0.5 m/s and U=0.7 m/s. The six selected sea states are denoted Irr1, Irr2 etc. The significant wave height (Hs) and peak period (Tp) is shown to increase for the runs. The wave steepness is characterised by a wave-height to wave-length ratio in the range $0.04 - 0.05$ or 1/20 - 1/26. The length of the time series is 1.5 hours. Tests in waves only were not executed, and isolated wave effects can therefore not be considered.

Table 6.4: Irregular runs, sea state parameters

| | Hs [m] | Tp [s] | Hs / $\lambda_p$ |
|---|---|---|---|
| Irr1 | 1.0 | 4.0 | $0.040 = 1/25$ |
| Irr2 | 1.5 | 4.5 | $0.047 \approx 1/22$ |
| Irr3 | 2.0 | 5.0 | $0.051 \approx 1/20$ |
| Irr4 | 2.5 | 6.0 | $0.045 \approx 1/22$ |
| Irr5 | 3.0 | 7.0 | $0.039 \approx 1/26$ |
| Irr6 | 4.0 | 8.0 | $0.040 = 1/25$ |

### 6.2.1 Total mean force

Calculated mean forces from the environmental loads in the irregular runs Irr1 - Irr6 are presented in figure 6.1. Values are also given in table 6.5. The current only cases (C1 and C2) are included in the plots to indicate the magnitude of current mean force versus total mean force. Hs [m] for the runs is also indicated.

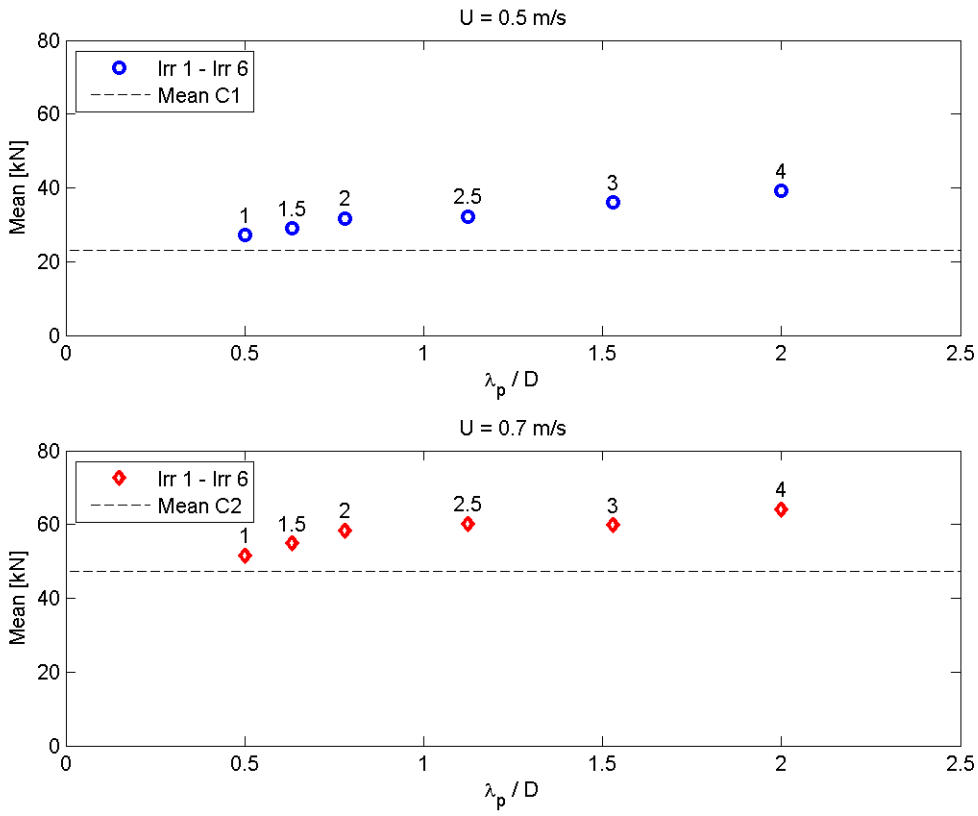


Figure 6.1: Total mean force in anchor lines from waves and current (Irr1-Irr6) for current velocities U=0.5m/s and U=0.7m/s. Hs [m] is indicated. Mean current force is included.

Table 6.5: Mean force [kN] in anchor line 1 (AL 1) and anchor line 2 (AL 2). $\overline{AL}$ is the average.

| | Sea state | | U=0.5 m/s | | | U=0.7 m/s | | |
|---|---|---|---|---|---|---|---|---|
| | Hs | Tp | AL 1 | AL 2 | $\overline{AL}$ | AL 1 | AL 2 | $\overline{AL}$ |
| Irr 1 | 1.0 | 4.0 | 26.8 | 27.5 | 27.1 | 53.0 | 50.1 | 51.6 |
| Irr 1 | 1.0 | 4.0 | 26.8 | 27.5 | 27.1 | 53.0 | 50.1 | 51.6 |
| Irr 2 | 1.5 | 4.5 | 28.3 | 29.6 | 29.0 | 56.1 | 53.5 | 54.8 |
| Irr 3 | 2.0 | 5.0 | 31.1 | 32.4 | 31.8 | 58.9 | 57.6 | 58.3 |
| Irr 4 | 2.5 | 6.0 | 31.1 | 33.1 | 32.1 | 60.5 | 59.8 | 60.2 |
| Irr 5 | 3.0 | 7.0 | 36.3 | 35.6 | 36.0 | 60.3 | 59.0 | 59.7 |
| Irr 6 | 4.0 | 8.0 | 39.6 | 38.7 | 39.2 | 64.5 | 63.6 | 64.1 |

From figure 6.1, it is observed that the total mean force in current and irregular waves increases with wave period. The total load increases with wave height and wave period. The mean load for current only condition is included in the figure and indicates that current force dominates the total mean force.

### 6.2.2 Mean dynamic force

It is seen from figure 6.1 that total mean force increases with wave length. The dynamic part of the mean load is investigated. In a dynamic analysis of e.g. marine risers, current is regarded a static load while wave effects are dynamic (Larsen 1990). The contributing force components are suggested as in equation (6.1). The total mean force is here divided into a static and dynamic mean force. The dynamic force is obtained by subtracting the current only force from the total mean force. However, due to the quadratic drag term, the current also contributes to a part of the mean dynamic force.

$$F_{DYN} = F_{TOT} - F_{STATIC} \tag{6.1}$$

where $F_{DYN}$ is the dynamic load from waves and currents, $F_{TOT}$ is the total load from waves and currents and $F_{STATIC}$ is assumed to be the static load from currents only. Mean dynamic force is presented in figure 6.2. Hs [m] for the runs in indicated in the figure.

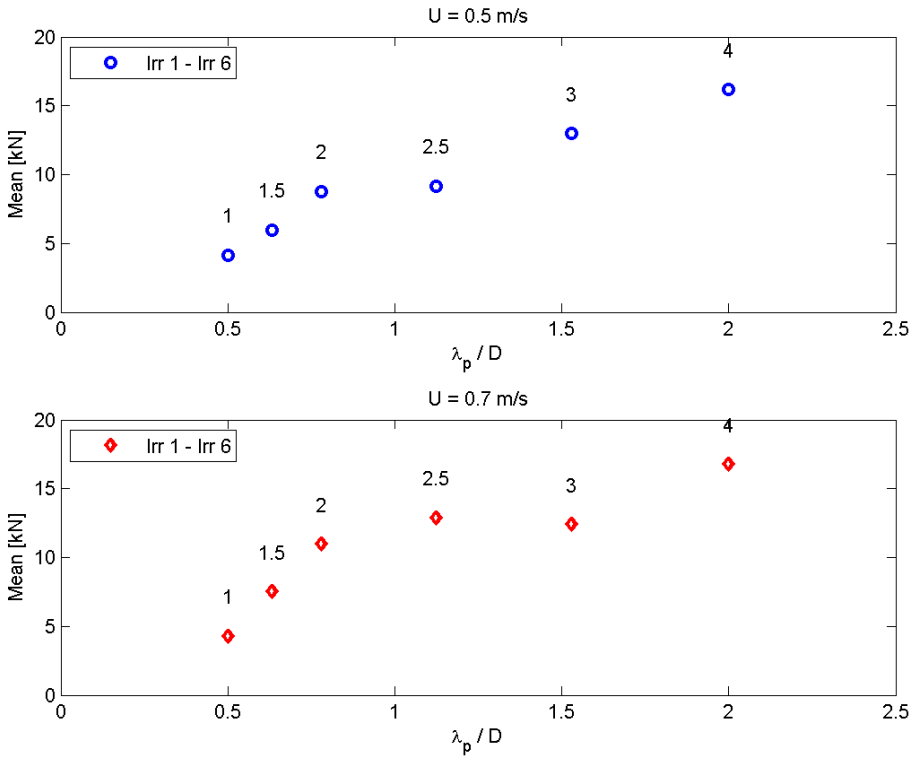


Figure 6.2: Mean dynamic force ($F_{DYN}$) in the anchor lines from waves and current, Irr1-Irr6 for U=0.5m/s and U=0.7m/s. Hs [m] for the runs is indicated

The wave parameters Hs, Tp and $\lambda_p$ are investigated with the aim of finding a correlation between the mean dynamic force and $\lambda_p$/D ratio.

Three hypothesis are tested:

1. Dynamic mean force increases linearly with $\lambda_p$/D for a constant wave steepness. This idea is adapted from Kristiansen & Faltinsen (2014), where this trend is observed for regular waves and current.

2. Dynamic mean force can be normalized with the ratio $u_w/U_\infty$, where $u_w$ is the horizontal wave particle velocity and $U_\infty$ current velocity.

3. Dynamic mean force can be scaled as added drag. A recommendation

from Grue (2014).

**1. Dynamic mean force increases linearly with $\lambda_p$/D for a constant wave steepness $Hs/\lambda_p$**

As listed in table 6.4, some of the runs have nearly the same wave steepness. The six irregular runs are divided into groups with Hs/$\lambda_p$-ratio of 1/25 and 1/22 respectively. Irr1, Irr5, and Irr6 are characterized by wave steepness 1/25. Irr2 and Irr4 are characterized by wave steepness 1/22. The data of dynamic mean force is fitted to a linear curve and presented in figure 6.3. The mean dynamic force for Hs/$\lambda_p$=1/22 is included.

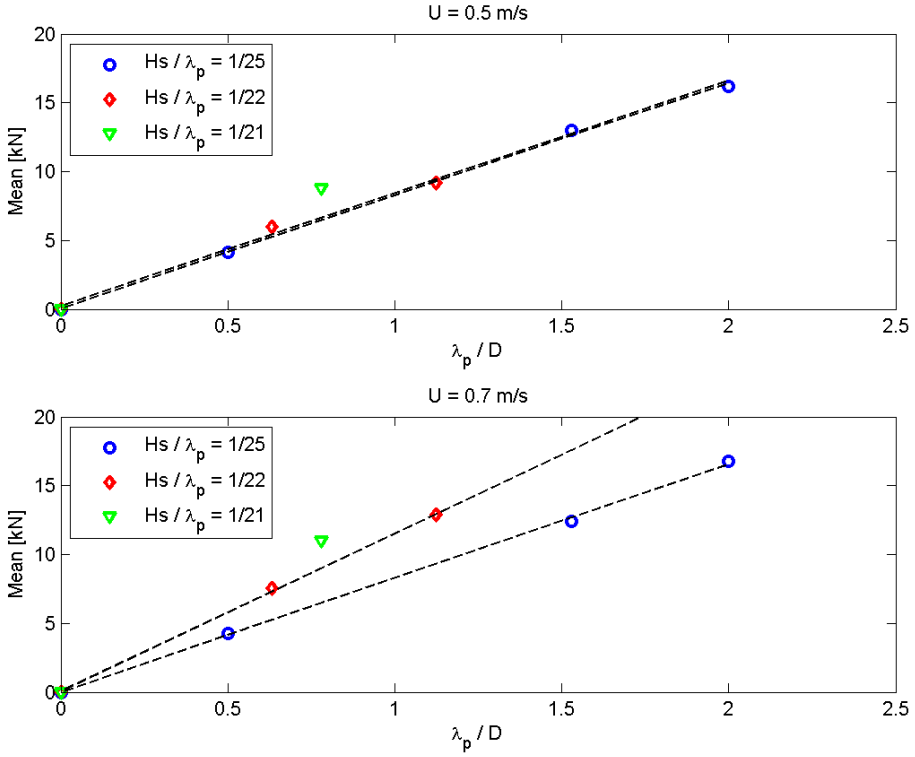


Figure 6.3: Curve fitting of mean dynamic force with constant Hs/$\lambda_p$

From figure 6.3 it is observed that the mean dynamic force tends to increase

linearly with $\lambda_p$/D for a constant wave steepness. The trend is seen for both current velocities U=0.5m/s and U=0.7m/s.

In the upper part of figure 6.3 it is observed that the lines for the steepnesses 1/25 and 1/22 coincides. In the lower part of figure 6.3, the slope of the linear curve seems to be steeper for steeper waves.

The linear trend of the mean dynamic force is also observed in Kristiansen & Faltinsen (2014). An approximate formula is suggested in 6.2 according to recommendations from Kristiansen (2014). It is a formula of the mean force for constant wave steepness. The estimate is plotted together with the experimental mean dynamic force in figure 6.4.

$$F_{TOT} = \frac{D}{8\pi}\rho C_D^0 g\epsilon^2 L\lambda + F_{STATIC} \tag{6.2}$$

D is the net cage diameter, $C_D^0$ is the drag coefficient as presented in table 6.3. It assumes initial net cage configuration in calm water. $\epsilon$ is the constant wave steepness and L is the depth of the net, which is set to the depth of the cylindrical net cage.

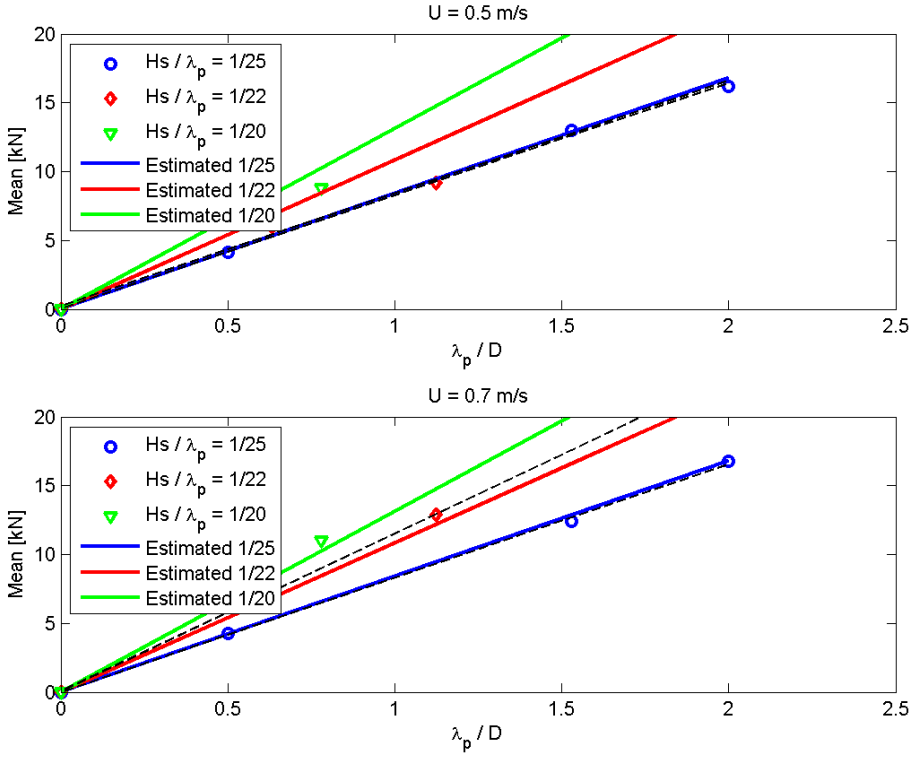


Figure 6.4: Experimental and empirical mean dynamic force with constant $\mathrm{Hs}/\lambda_p$

Figure 6.4 shows the experimental results included the estimated mean dynamic load from equation (6.2). An agreement between the empirical and experimental mean dynamic force is observed for $\mathrm{Hs}/\lambda_p = 1/25$ for both current velocities. This may indicate that the mean dynamic force for this wave steepness is not significantly affected by the currents. However, only a limited number of measurements are performed and further investigations are required. A fairly good agreement between the estimated and experimental mean dynamic forces is seen for all wave steepnesses for the current velocity U=0.7m/s. This is not observed for the current velocity U=0.5m/s.

### 2. Dynamic mean force and relative velocity ($\frac{u_w}{U_\infty}$)

It is assumed that the horizontal loads are the main contributor to the mean loads. The theoretical drag force is a function of ${U_{rel}}^2$, which includes a coupling term between the current and wave particle velocity. The horizontal water velocity can be described as in equation 6.3. The ratio between wave particle velocity and current velocity are examined and presented in figure 6.5.

$$u_w = \frac{\partial \phi}{\partial x} = \omega \zeta_a e^{kz} \sin(\omega t - kx) \propto \omega \zeta_a \tag{6.3}$$

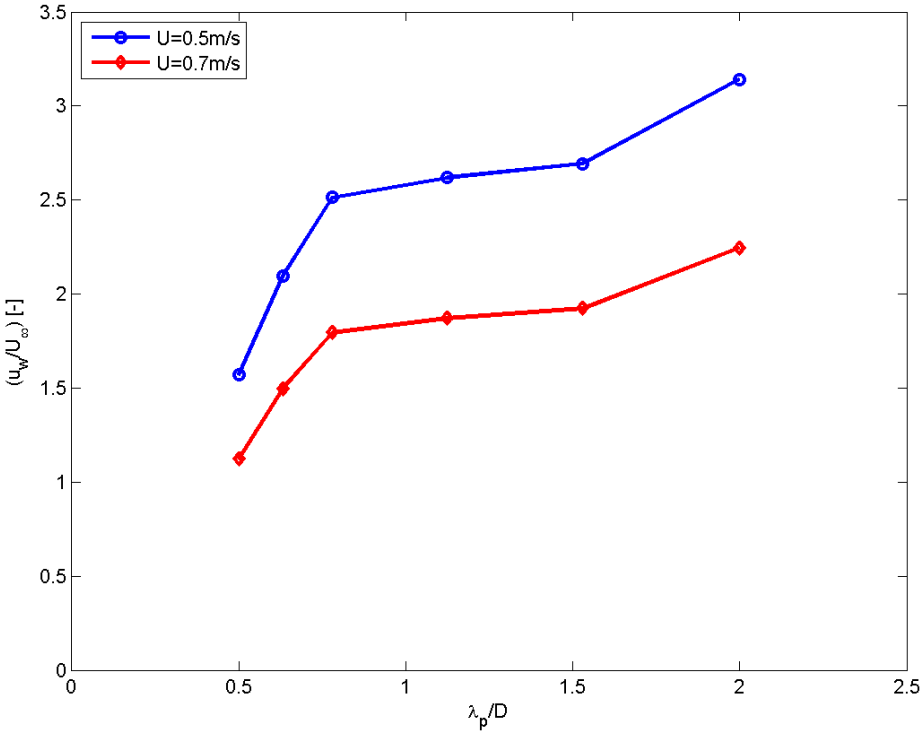


Figure 6.5: Ratio between wave particle velocity $u_w$ and current velocity $U_\infty$.

Figure 6.5 shows the trend of the ratio between $u_w$ and $U_\infty$, which is seen to

increase with wave length. This has similarities to the trend of mean dynamic force presented in figure 6.2. This may indicate that the dynamic force can be proportional to this ratio. The mean dynamic force is normalized with the ratio and also the ratio squared. When mean dynamic force is normalized with the squared ratio, a constant value is found for the mean dynamic load, as presented in figure 6.6.

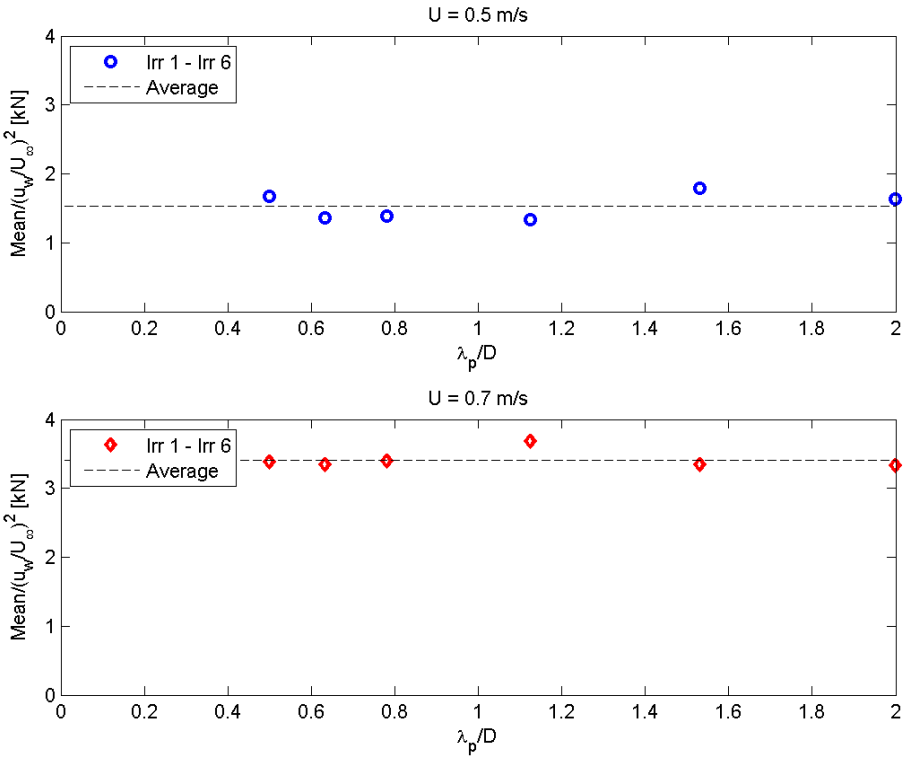


Figure 6.6: Mean dynamic force normalized with $(\frac{u_w}{U_\infty})^2$.

In figure 6.6, the mean dynamic load is normalized to the squared relative velocity between horizontal wave velocity and current velocity. A constant value is obtained for both U=0.5m/s and U=0.7m/s. This indicates that the mean force can be normalized with $\omega^2{\zeta_a}^2$. The result requires further investigation, due to that only a limited test conditions are examined in this analysis.

It is also noticed that in these considerations, the velocity of the net cage is not accounted for. Net cage velocity might alter the relative velocity and further investigations are required.

### 3. Dynamic mean force scaled as added drag

According to (Faltinsen 1990), added resistance is the same as the longitudinal drift-force component. He suggests the formula:

$$\sigma_{AW} = \frac{R_{AW}}{\rho g {\zeta_a}^2 B^2/L} \tag{6.4}$$

For the gravity net cage, $B^2/L$ is D, and the added resistance is considered as added drag according to recommendations from Grue (2014).

$$\sigma_{F_{DYN}} = \frac{F_{DYN}}{\rho g {\zeta_a}^2 D} \tag{6.5}$$

The dimensionless added drag of the net cage is presented in figure 6.7. The added drag from the test conditions in regular waves and currents are also included to examine the trend for regular waves.

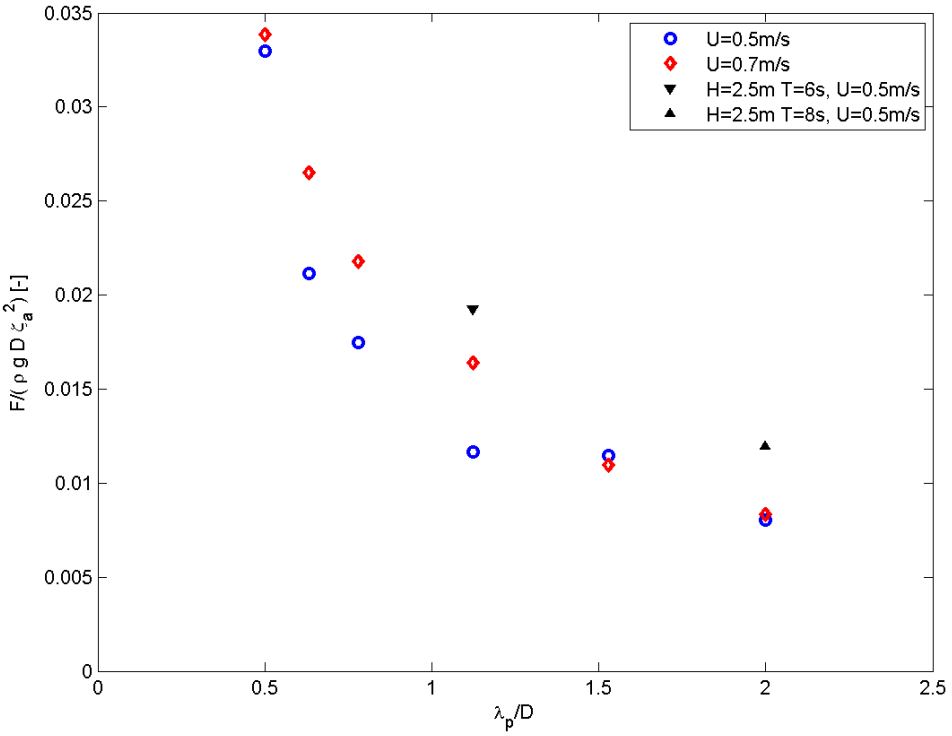


Figure 6.7: Wavelength dependence of added drag, $F_{DYN}$, when dynamic mean force is scaled according to equation 6.5

In figure 6.7, it is observed that the scaled added drag decrease with increased wave length. The scaling of added drag seems to have a similar trend for the irregular measurements and the regular measurements (CW1 and CW2), although the value differs significantly.

### Viscous effects on mean wave forces

When viscous wave drift forces become small, viscous effects may contribute to drift forces (Faltinsen 1990). The effect is of third order, which means it is proportional to the cube of the wave amplitudes in regular waves. A different scale $\propto {\zeta_a}^3$ is obtained when viscous effects become more and more important with increasing wave amplitude (Faltinsen 1990). According to

the dominance of drag forces on the gravity net cage, this correlation is examined. In this case $C_D$ is set to 1 since it is only a scaling and do not change for the investigated dynamic mean loads.

$$F_{DYN} = \frac{2}{3\pi}\rho C_D \omega^2 {\zeta_a}^3 \tag{6.6}$$

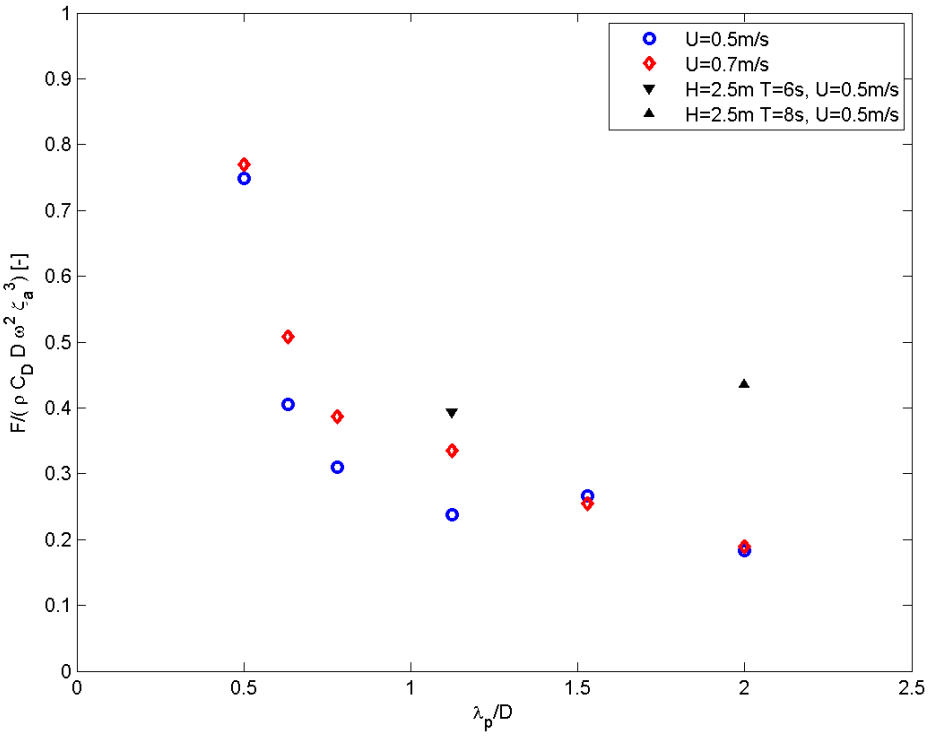


Figure 6.8: Wavelength dependence of added drag, $F_{DYN}$, when dynamic mean force is scaled as equation 6.6

From figure 6.8 it is seen that the scaled added drag decrease with wave length. The dynamic mean loads from regular waves and currents are included, and the trends do not seem to agree.

In figure 6.7 and 6.8, the suggested scaled added drag for 6 irregular tests and two regular tests is presented. In figure 6.7 it is observed a similar trend

for added drag in both irregular and regular test conditions. A similar trend for irregular and regular tested condition is not clearly seen in figure 6.8, and indicates that $\zeta_a^2$ can be a preferred scale for the mean dynamic force.

## 6.3 Total force

Figure 6.9 presents a portion of the time series of the total force for Irr4. Total force, low frequency force and the wave elevation are included. Note that the wave elevation is measured 80m to the side of the net cage. Long crested waves were applied in the conducted experiment.

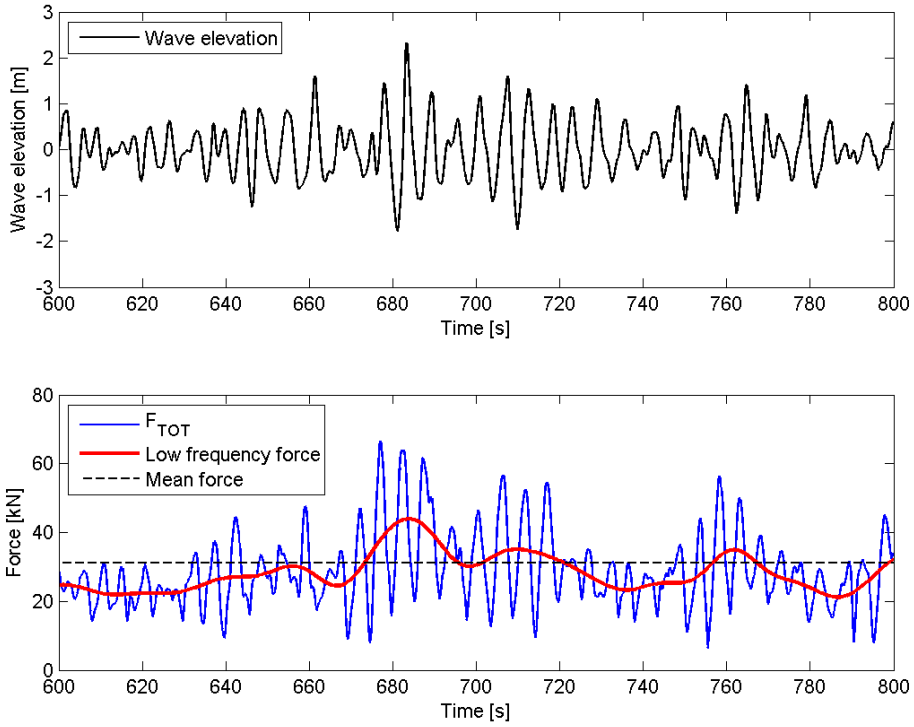


Figure 6.9: Time series of total mooring line force, slow frequency force and wave elevation for Irr4

By visual inspection of figure 6.9, a correlation between total force from waves and currents and the wave elevation is observed. The low frequency force is obtained by use of a band pass filter received from Kristiansen (2014). The upper cut-off frequency, $f_u$, was decided on 0.05Hz after a sensitivity study. Details of this study is presented in appendix C.

# Chapter 7

# Validation of FhSim

In this chapter, predicted mooring line forces from FhSim is compared to experimental results and fishFarm. The validation study is divided into two parts since it was necessary to perform two independent comparison studies.

In part I, a validation study of system A is performed. In part II, a validation study of system B is performed. One should bare in mind, that the two systems differ in mooring line system complexity, net cage and bottom ring design as well as in over all dimensions. Based on this, the loads from the two systems can not be compared directly.

The main focus in on the agreement of the mean force, and the environmental conditions are limited to current and regular waves.

## 7.1 Part I: System A simulated in FhSim

Results in this section are based on simulations of system A in FhSim, see figure 5.3 in section 5.3.1. The coherence between simulated results and experimental results presented in section 6.1 is examined.

### 7.1.1 Simulated results

In table 7.1, the calculated mean force in bridle, buoy chains and anchor lines from 6 simulations are presented. Note that the pretension is only subtracted in the cases W1, W2, CW1 and CW2. Uncertainties in the numerical solver were detected by visual inspection of the force time series as illustrated in figure 7.1. It was decided to repeat the simulations in order to detect the precision error. The ensemble average is denoted by $\overline{X}$, the standard deviation by $S_X$ and the precision limit by $P_X$ .

Table 7.1: Mean force from 6 simulations. Ensemble average ($\overline{X}$), standard deviation ($S_X$), precision limit ($P_X$) and uncertainty (UN) are presented

| Case | Simulations | | | | | | Statistics | | | |
|---|---|---|---|---|---|---|---|---|---|---|
| | 1 | 2 | 3 | 4 | 5 | 6 | $\overline{X}$ | $S_X$ | $P_X$ | UN |
| Bridle | | | | | | | | | | |
| C1 | 20.6 | 17.9 | 19.6 | 20.0 | 20.0 | 20.7 | 19.8 | 1.0 | 2.7 | 5.5% |
| C2 | 37.2 | 31.8 | 31.1 | 31.6 | 34.9 | 33.9 | 33.4 | 2.4 | 6.1 | 7.4% |
| W1 | 2.4 | 2.6 | 2.4 | 2.4 | 2.4 | 2.4 | 2.4 | 0.1 | 0.3 | 4.5% |
| W2 | 0.9 | 0.9 | 0.9 | 0.9 | 0.9 | 1.0 | 0.9 | 0.0 | 0.1 | 4.2% |
| CW1 | 33.5 | 38.0 | 33.9 | 38.1 | 33.7 | 35.2 | 35.4 | 2.1 | 5.4 | 6.2% |
| CW2 | 28.3 | 28.4 | 26.6 | 28.4 | 35.0 | 28.2 | 29.2 | 3.0 | 7.7 | 10.8% |
| Buoy | | | | | | | | | | |
| C1 | 15.6 | 14.3 | 15.1 | 15.3 | 15.4 | 15.7 | 15.2 | 0.5 | 1.3 | 3.6% |
| C2 | 25.5 | 22.9 | 22.6 | 22.8 | 24.5 | 23.9 | 23.7 | 1.1 | 2.9 | 5.0% |
| W1 | 3.2 | 3.3 | 3.2 | 3.2 | 3.2 | 3.2 | 3.2 | 0.1 | 0.1 | 1.8% |
| W2 | 2.8 | 2.8 | 2.8 | 2.8 | 2.8 | 2.8 | 2.8 | 0.0 | 0.0 | 0.5% |
| CW1 | 21.3 | 23.3 | 21.7 | 23.3 | 21.3 | 21.9 | 22.1 | 0.95 | 2.4 | 4.5% |
| CW2 | 18.2 | 18.2 | 17.3 | 18.2 | 21.1 | 18.1 | 18.5 | 1.3 | 3.3 | 7.4% |
| Anchor line | | | | | | | | | | |
| C1 | 37.3 | 33.5 | 35.8 | 36.5 | 36.5 | 37.6 | 36.2 | 1.5 | 3.8 | 4.3% |
| C2 | 68.3 | 60.1 | 59.2 | 59.9 | 65.0 | 63.2 | 62.6 | 3.6 | 9.3 | 6.0% |
| W1 | 6.2 | 6.5 | 6.1 | 6.1 | 6.1 | 6.1 | 6.2 | 0.1 | 0.4 | 2.4% |
| W2 | 4.8 | 4.8 | 4.7 | 4.7 | 4.8 | 4.8 | 4.8 | 0.0 | 0.1 | 1.1% |
| CW1 | 59.0 | 66.3 | 60.4 | 66.3 | 59.3 | 61.4 | 62.1 | 3.4 | 8.7 | 5.8% |
| CW2 | 51.0 | 51.1 | 48.3 | 51.1 | 60.5 | 50.7 | 52.1 | 4.2 | 10.8 | 8.5% |

From table 7.1 it is observed that the computed mean force varies for the repeated simulations in all structural parts of the mooring system. The precision limit and uncertainty is larger in the cases with current than the wave only cases (W1 and W2). The uncertainty calculations show an upper limit of 10.8 % in the bridle exposed to current and waves (CW2). This uncertainty level is somewhat higher than one would expect for this type of simulations (Steen 2014).

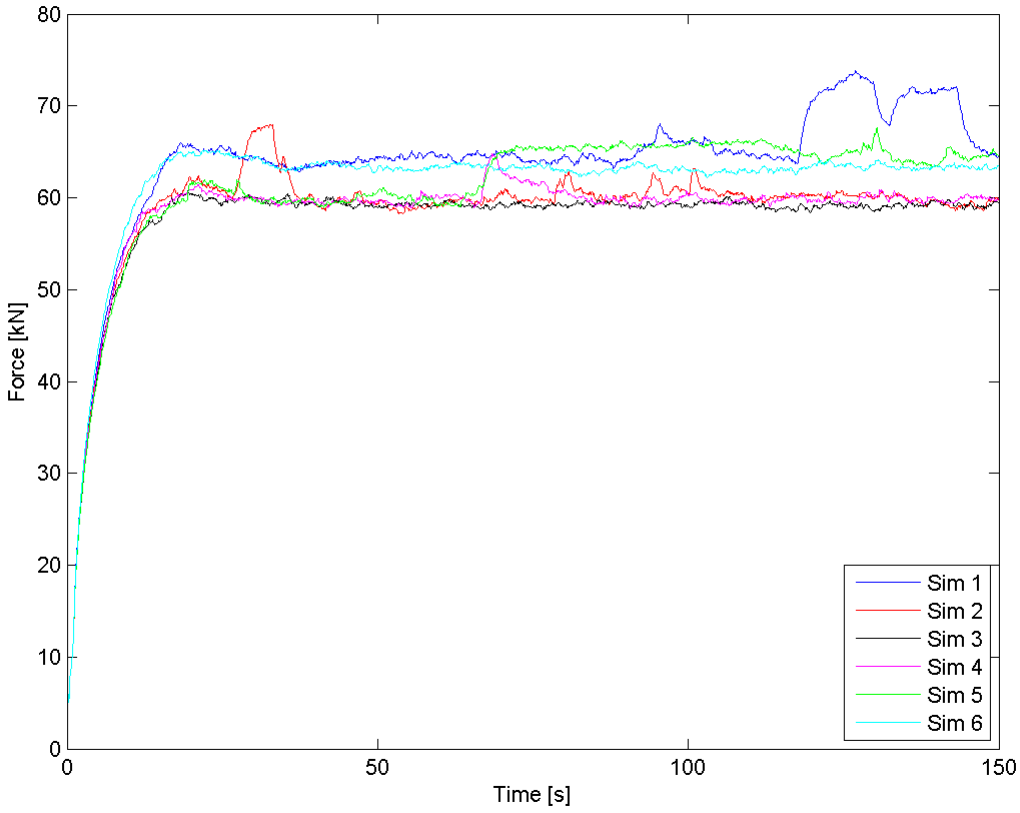


Figure 7.1: Time series of force in anchor line 1 for environmental condition C2 (U=0.7m/s). 6 repeated simulations executed for the identical input file

### 7.1.2 Numerical uncertainty

As mentioned, uncertainties in the numerical solver for the model of system A were detected from simulated results in FhSim. Figure 7.1 shows the time series of six repeated simulations in current only (C2). Examples of time series for the cases W1 and C1 are included in appendix D.3. Significant jumps or peaks in the steady state part of the time series are observed. These are unexpected results and alter the evaluation of mean force from the simulations. In order to determine how much the deviations affect the results, the precision limit of the simulations is examined.

#### Precision limit and uncertainty

Replication of the simulations can be used to determine the precision error. Precision error is related to the random error associated with the simulations. Repeated simulations were executed for the identical input file, creating a sample of six calculated mean forces.

The 6 calculated mean forces are described by the ensemble average $\overline{X}$ and standard deviation $S_X$. The calculation of precision error is performed according to (Steen 2012).

It is assumed that the sample of mean forces follows the student-t-distribution and a confidence interval of 95% is assumed. The precision limit and the associated uncertainty are calculated according to:

$$\begin{aligned} P_X &= tS_X \\ Uncertainty &= \frac{t\ S_X}{\sqrt{N}\ \overline{X}} \end{aligned} \tag{7.1}$$

where $t$ is calculated in excel from the function $TINV(1-0.95; N-1)$ and found to be 2.57. $F^{-1}$ is a function of degrees of freedom $N-1$, which is 5 in this case. $\gamma$ is the confidence interval of 95%.

### Comparison to Endresen et al. (2014)

To make sure the simulated results in the present thesis were reliable, a comparison was made to results in Endresen et al. (2014), where a validation study of FhSim of the similar system is presented. The applied input file in this thesis is identical to the input file used for the simulations in the paper. As a starting point, it was expected to obtain similar mean force computation as Endresen et al. (2014). By comparing the presented simulated results, errors connected to the simulations were clarified. The study was time consuming and included a check of the input file, the post processing routines, and also a second version of FhSim. The whole study is included in appendix D.

The main outcomes of the study were:

- The input file utilized in this work is similar as used in Endresen et al. (2014).
- The developed post processing routines extract the relevant forces.
- Executing the analysis in an older version of FhSim do not affect the predicted results.
- When comparing the force only in one mooring line, the pretension must be subtracted. By use of this procedure, the load caused by environmental loads is isolated

### Pretension in mooring lines

In order to compare the mooring line loads for two systems, similarity in the mooring system geometry and structural properties are required. The particular interest is to determine the force contribution from the environmental loads on the mooring line loads.

When the net cage is in its initial configuration in calm water, there will be pretension in mooring line loads. The pretension varies from experimental model to simulated model, due to small modelling differences of the mooring line geometry and stiffness properties. In order to isolate the effect from environmental loads, the pretension should be subtracted.

When dimensioning the mooring lines, the total capacity should be the sum of environmental loads and the pretension.

### 7.1.3 Simulations compared to experimental results and validation of FhSim

The purpose of a validation study is to verify that the numerical model represents the physical reality in an adequate way. The simulated results of system A are compared to experimental results obtained in section 6.1. The ensemble average of the repeated simulations is used in the comparative study.

The comparison of the mean forces is presented in table 7.2, where simulated results are denoted by $\overline{X}$ and experimental results are denoted by Exp. The discrepancy between the experimental and simulated mean forces is presented as percentage deviation from the experimental results. Note that the pretension is subtracted in all cases.

Table 7.2: Ensemble average of mean force [kN] for simulations 1-6 compared to experimental results. The pretension is subtracted in all cases.

| | Average bridles | | | Buoy chain | | | Anchor line | | |
|---|---|---|---|---|---|---|---|---|---|
| | Exp | $\overline{X}$ | % | Exp | $\overline{X}$ | % | Exp | $\overline{X}$ | % |
| C1 | 23.1 | 18.9 | -18.1 | 8.3 | 11.7 | 41.5 | 23.0 | 32.8 | 42.7 |
| C2 | 40.1 | 32.6 | -18.9 | 17.0 | 20.1 | 18.4 | 47.3 | 59.2 | 25.2 |
| W1 | 7.5 | 2.4 | -67.6 | 2.8 | 3.2 | 16.9 | 8.0 | 6.2 | -23.0 |
| W2 | 2.3 | 0.9 | -60.0 | 1.3 | 2.8 | 112.7 | 3.5 | 4.8 | 35.9 |
| CW1 | 32.6 | 35.4 | 9.0 | 15.5 | 22.1 | 43.0 | 38.1 | 62.1 | 63.0 |
| CW2 | 28.7 | 29.2 | 2.0 | 12.3 | 18.5 | 50.0 | 32.4 | 52.1 | 61.0 |

When considering the mean force in the buoy chain and the anchor line in table 7.2, it is seen that FhSim ($\overline{X}$) overestimates the mean force compared to the experiments (Exp). An exception is seen for the environmental condition W1, where the simulation underestimates for the anchor line force. In the bridles, the mean force is generally underestimated.

The anchor line force in C1 and C2 is evaluated. From the simulated results in

current only condition, it will be shown in section 7.2.1, that FhSim slightly overestimate the mean force for increased current velocity for a different system. In table 7.2, the percentage deviation between the experimental and simulated results are 40.7% and 22%, respectively, which is the opposite to what expected.

From the simulated results of anchor line force in combined currents and waves (CW1 and CW2), it is observed that FhSim overestimates the mean load by 61-63 % compared to the experiments.

### 7.1.4 Error analysis

Possible sources of errors are listed in order to point at elements which might explain the deviations between experimental and predicted results. Errors are divided into systematic errors (bias) and random errors (precision) (Steen 2012). There are errors connected to both the experimental and the numerical mean force results.

#### Experimental error

- From the experimental results in section 6.1, it is seen that mean force is dominated by current. For an accurate force measurement, a constant current velocity is required and the current in the ocean basin is known to fluctuate. The current profile in the ocean basin can also vary with depth. Variations in the current velocity and profile might have influenced the accuracy of the force measurements in the anchor lines.
- The intention of the experiments was primarily to study the overall net cage behaviour in large current and waves. Measurements for validation purposes were of secondary importance. Correct pretension and a symmetric initial load distribution in the mooring line system might have affected the net cage behaviour and the load distribution throughout the mooring line system.
- The net cage is dominated by drag forces. The global load and thus the measured anchor line forces depend on the dimensions of the physical

twines. There might be uncertainties connected to the Froude scaling of the net mesh.

- In the performed experiment, springs were inserted in the mooring lines in order to measure the force. The force was measured only in the front part of the mooring system. The installed instrumentation might have altered the the elastic stiffness, and affected the force distribution in the mooring system.
- In order to distinguish between precision and systematic errors, the replication level must be considered. Precision error can be covered by repetition of the tests. In this experiment, repeated tests were not performed, and the precision limit is unknown.

**Numerical error**

- The modelled mooring lines of system A consist of several interconnected ropes and is a complex system. To ensure a similar load distribution in both the experimental and the numerical model, similar modelling properties in terms of stiffness characteristics and pretension are required. Differences in these properties between simulated and tested model, may alter the load predictions.
- Uncertainty and instability in the applied numerical solver. The estimation of precision limit from repeated simulations indicates a variation in simulated results for the numerical program.
- The implemented hydrodynamic load model, and its ability to predict the environmental loads precisely on all the comprising parts of the system. Both how the load model accounts for the ambient current and the oscillating wave velocity in the force model impacts the total load prediction. Introduction of waves complicates the water flow, and the ability of the numerical program to include this in the force computations impact the load prediction.
- Human errors while generating the input file and parameters for environmental conditions leads to wrong output. However this is normally limited by extent use of computed programs.

### 7.1.5 Discussion

In the evaluation of coherence between experimental data and model prediction, one must account for the error and uncertainties connected to both simulations and experiments (Thacker et al. 2004). The particular accuracy level also influence whether the agreement can be characterized as acceptable. From repetition of simulations, a precision limit of the simulated results is determined. The experimental results are not found to be within the precision limit of the numerical results. Due to lack of repeated tests, the experimental precision limit is not determined, but is assumed to be approximately 10 % (Steen 2014).

From the comparison of the rather limited amount of data in regular waves and current for system A, a percentage deviation of 22%-63% is found between experimental and predicted mean loads. An exception is the wave only condition, W1, where FhSim underestimates with 23%.

Model validation assessment determines to what degree a model is an accurate representation of the real world (Thacker et al. 2004). The model should be evaluated from the perspective of its intended use. In this thesis, the intention is to predict mooring line loads in large currents and waves. For a fish farm, the accidental loads should be evaluated in the mooring line carrying the largest load (Standard 2009). The largest combination of current and waves is considered as the dimensioning load case. For use in design assessment, it is important that FhSim compute accurate loads in a combined current and wave condition.

For the investigated environmental conditions in currents and waves, the mean load is found to be significantly overestimated with approximately 61-63%. For a software assessing mooring line loads, one would enhance more accurate prediction of loads. Ideally, the software should be able to predict the loads accurately and later consider safety factors to determine the design load.

In Thacker et al. (2004), they point out that for a system comprised of several subsystems, the approach of validating the entire system can be problematic. If poor agreement between prediction and experiment is obtained, it can be difficult to isolate which subsystem is responsible for the discrepancy. Even if good agreement between prediction and experiment is observed, it is still

possible that the model quality could be poor because of error cancellation among the subsystem models.

In the attempted validation study, there are several open questions of what factors that influence the deviations between the experimental and predicted result. Errors in the simulations might be caused by direct modelling errors. The complexity of the mooring configuration of system A makes it difficult to detect the error and improve the model.

Further validation studies are needed. Due to lack of a wide set of experimental results for system A in current and regular waves, a net cage with a simplified mooring system will be considered. By reducing the mooring line system, modelling errors connected to the lines are reduced. The further work considers system B. This model can be simulated in two of the available numerical software. Existing experimental results presented in Kristiansen & Faltinsen (2014) for a range of environmental conditions are used in the comparative study.

## 7.2 Part II: System B simulated in FhSim and fishFarm

In this section, simulations of system B are performed in FhSim and fishFarm in order to compare the numerical programs in terms of mean global load estimation. An overview of the system is presented in figure 5.4. For this model, the mooring line system is simplified and consists only of the bridles. The considered gravity net cage is modelled without a bottom and the bottom ring is discretized. Both numerical solvers support the analysis of this gravity net cage design in current and regular waves.

Table 7.3 gives an overview of the simulated current and wave conditions. The simulated results are compared to experimental results in Kristiansen & Faltinsen (2012*b*). For the considered model, a reasonable agreement between the experiments and fishFarm is presented in Kristiansen & Faltinsen (2012*b*). Hence, FhSim can be compared to fishFarm in order to evaluate whether the numerical computations are reliable.

Table 7.3: Simulation matrix

| Environmental condition | U [m/s] | Wave steepness |
|---|---|---|
| Current only | 0.1-1.0 | - |
| Waves and current | 0.5 | 1/30, 1/15 |
| | 0.7 | 1/30, 1/15 |

### 7.2.1 Current only

Figure 7.2 shows the global horizontal mean load on the net cage for current velocities in the range 0-1.0m/s. In table 7.4, the mean load for the cases U=0.5m/s, U=0.7m/s and U=1.0m/s are listed, and the two numerical solvers compared to the experimental results. Percentage discrepancy to experimental results is given in the parenthesis.

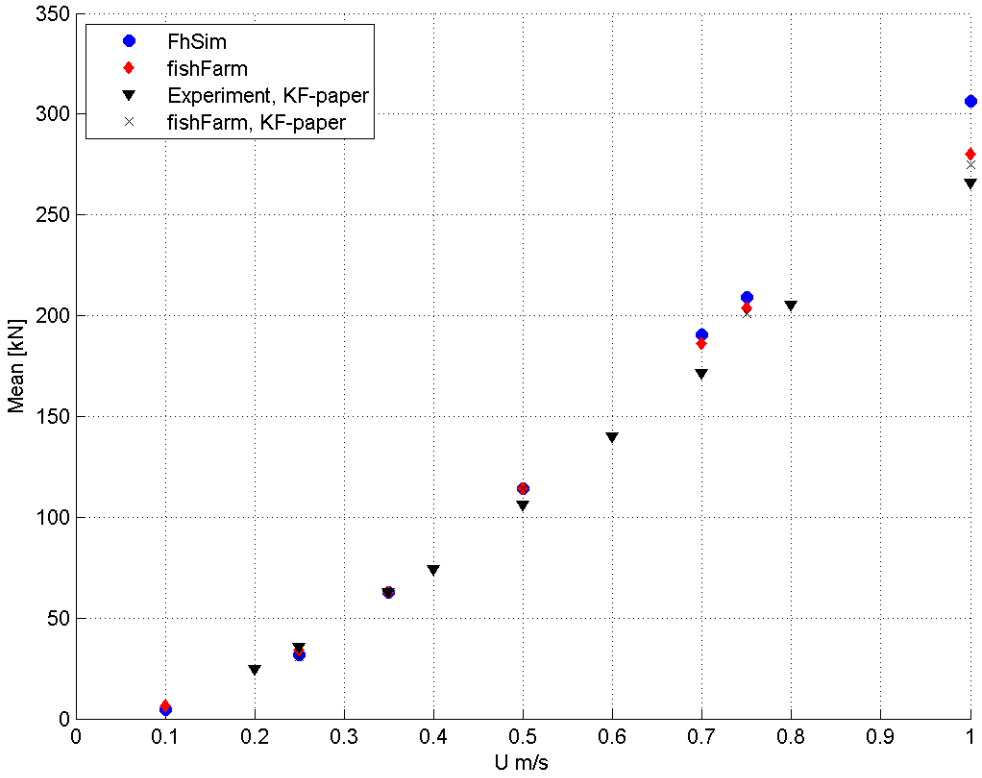


Figure 7.2: Mean horizontal force in current only. Computations from FhSim and fishFarm. Experimental and simulated results from Kristiansen & Faltinsen (2012*b*) (KF-paper) are included.

Table 7.4: Mean force from experiment, FhSim and fishFarm in current only condition, U=0.5m/s, U=0.7m/s and U=1.0m/s

| U [m/s] | Exp | FhSim | fishFarm |
|---|---|---|---|
| 0.5 | 105.9 | 114.0 (7%) | 114.3 (7.9%) |
| 0.7 | 171.5 | 190.5 (11%) | 186.3 (8.6%) |
| 1.0 | 266.0 | 306.3 (15%) | 280.3 (5.0%) |

It is observed in figure 7.2 that the horizontal mean force increases with the current velocity. The trend is stronger than linear, but weaker than

quadratic. A comparison of the computed forces shows that both FhSim and fishFarm compute fairly similar mean loads for current velocities up to 0.5 m/s. Above 0.7m/s, FhSim tends to compute slightly more conservative mean forces compared to fishFarm. For U=1.0 FhSim significantly overpredict horizontal mean force compared to fishFarm.

When comparing the predicted results to the experimental results in Kristiansen & Faltinsen (2012*b*), it is observed a fairly good agreement for current velocities below 0.35 m/s. Above U=0.5m/s, the simulated results are seen to be conservative and overestimate the mean loads slightly. fishFarm is somewhat closer to the experimental values than FhSim, especially for U=1.0m/s. One can say that for current velocities up to U=0.7m/s, both FhSim and fishFarm predict acceptable mean loads for the

In table 7.4, the percentage deviation between FhSim and experimental results for large current velocities is listed. The discrepancy level is observed to be far beyond the levels found for current only cases in section 7.1.3. considered model.

### 7.2.2 Current and waves

In this section, simulated result of the considered gravity net cage in currents and waves are presented. Global horizontal mean force is predicted from FhSim and fishFarm for two different wave steepnesses and the current velocities U=0.5m/s and U=0.7m/s. Mean load is investigated for increased wave length and wave height. The results are presented in figure 7.3 and 7.4. Simulated and experimental results from Kristiansen & Faltinsen (2012*b*) are included in the figure for illustrative purposes.

It is noticed that the results from Kristiansen & Faltinsen (2012*b*) in waves and current, constitute of mean loads only in front and aft mooring line, see figure 5.4 for the mooring line configuration. The mean load presented here is the total horizontal mean force for the system, which is the summed force from all mooring lines. The differences between the values found in Kristiansen & Faltinsen (2012*b*) and the simulated values is explained by the forces carried by the side mooring lines.

The reason for not computing only the fore and aft mean mooring line load in the present work, is that the model in FhSim does not include a spring in the

front mooring line. Thus, the front mooring line will absorb nearly the total horizontal mean load. Despite these modelling differences, it is assumed that the computation of the horizontal mean load is not significantly affected.

Figure 7.3 presents the global horizontal mean force from FhSim and fishFarm in currents and waves. The waves are characterized by a wave steepness of 1/30, which can be considered as medium steep waves. Experimental and simulated results from Kristiansen & Faltinsen (2012*b*) are included to compare the trends of mean force for increasing wave length.

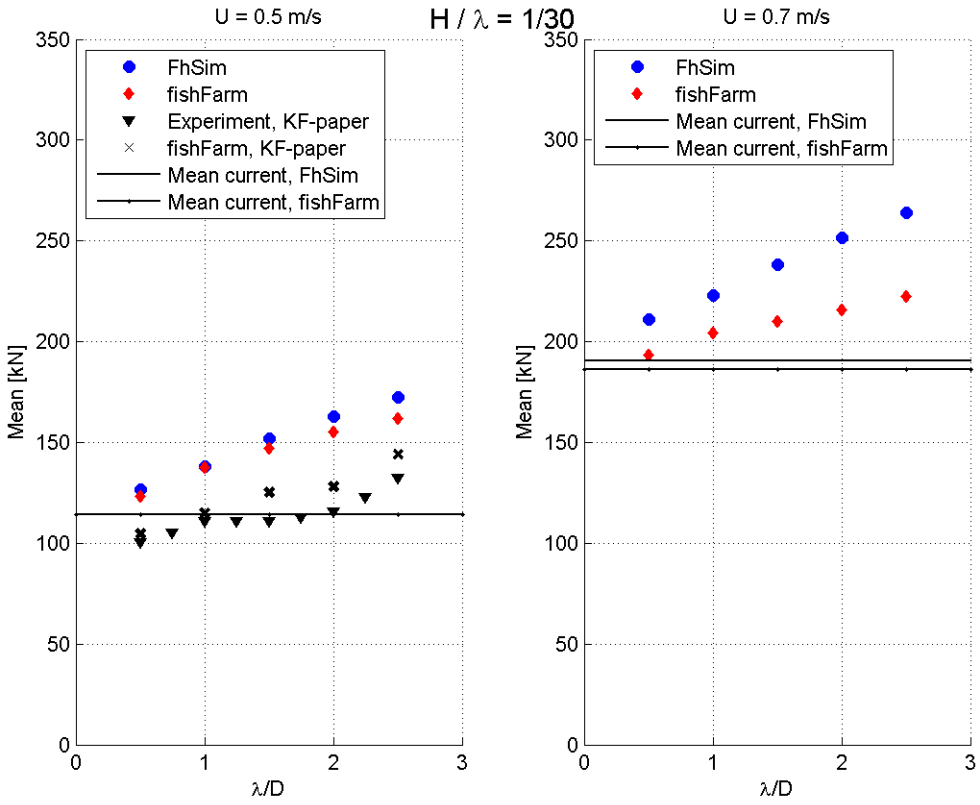


Figure 7.3: Mean horizontal force. $H/\lambda = 1/30$ Results from (Kristiansen & Faltinsen 2012*b*) (TK-paper) is only the sum of force in front and aft mooring line

From figure 7.3 it is observed that total mean force tends to increase linearly

with $\lambda$/D for both FhSim and fishFarm. It is also observed that fishFarm and FhSim compute fairly similar horizontal mean force for U=0.5m/s. A slight discrepancy is observed for increased wave length and wave height. From the simulated results with the current current velocity of U=0.7m/s, it is observed that FhSim overestimates mean load compared to fishFarm.

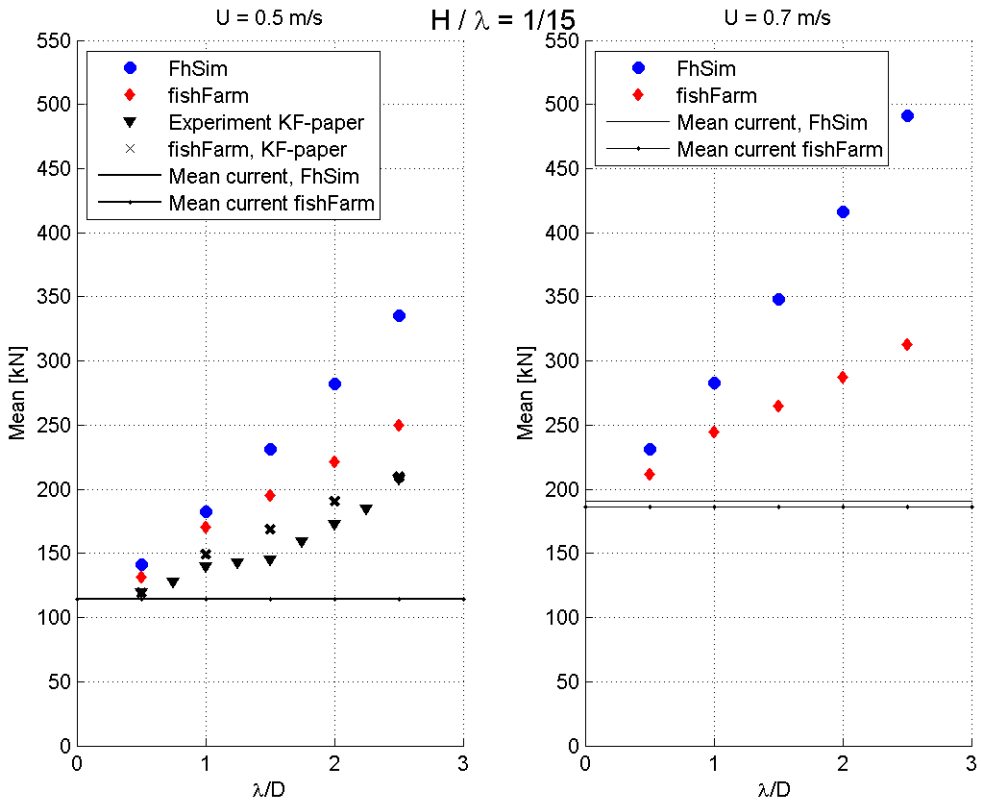


Figure 7.4: Mean horizontal force. H/$\lambda$ = 1/15

In figure 7.4, the mean load is computed for steeper waves, characterized by H/$\lambda$=1/15. It is observed that mean force increases nearly linear with $\lambda$/D, but the slope of mean force computed by FhSim is steeper than for fishFarm. It is seen that FhSim increasingly overestimates mean loads compared to fishFarm for increased wave length.

**Mean dynamic load**

As presented in connection to the experimental results in section 6.2.2, the total mean force subtracted the mean load caused by current is assumed to be the mean dynamic force $F_{DYN}$. The dynamic force includes forces from both waves and current. In section 6.2.2 part 2, the mean dynamic force was normalized with the ratio $(\frac{u_w}{U_\infty})^2$ or scaled as added drag. These hypothesis are tested for the dynamic mean force predicted from FhSim and fishFarm. The results are included in appendix E, and used as background information in the following discussion.

### 7.2.3 Discussion

A net cage with a simplified mooring system is simulated in FhSim and fishFarm. The global horizontal mean forces in mooring lines are compared. The numerical comparison study shows that:

- In current only, both programs compute fairly similar mean load for current velocities up to 0.5m/s. For current velocities above this, FhSim is observed to slightly overestimate mean loads compared to fishFarm.
- The computed mean load is overestimated compared to existing experiments for both programs for current velocities above U=0.5m/s.
- Mean loads in regular waves and current tends to increase linearly with wave height and wave length for both FhSim and fishFarm. The mean load is dominated by current.
- In waves and current, FhSim and fishFarm compute fairly similar results for current velocity U=0.5 m/s and a constant wave steepness of 1/30. A slight deviation in the mean load prediction is observed between the two programs.
- In waves characterized by the constant wave steepness 1/15 and current, a discrepancy in mean load computation between FhSim and fishFarm is observed. The discrepancy increases for larger wave lengths, for both current velocity U=0.5m/s and U=0.7m/s. This indicates that FhSim significantly overestimates mean loads for steep waves and currents compared to fishFarm. The increased current velocity may also

contribute to the increased mean load.

The similar floater load model is implemented in both FhSim and fishFarm. The reason for the deviations in horizontal mean loads can be explained by the computed loads on the net cage. Because of this, the discussion is focused around net load computation.

The overestimation by FhSim can be explained by the implemented load model which shows limitations for large water flow velocities. FhSim applies a Morison type force model, while fishFarm applies a screen type model as discussed in section 3.3.5. Predicting the drag force on a net cage by summing up the force contribution from all twines, as in a Morison type load model, may considerably overpredict the drag force (Lader & Fredheim 2006). The drag model based on Morisons equation cannot be justified for inflow angles larger than 45 ° (Kristiansen & Faltinsen 2012*a*). When the net is deflected, the projected area is reduced, and the load model is not capable to adequately account for this.

In currents and waves, the deviations between the simulated results from FhSim and fishFarm is observed to increase with wave height and wave length. It is seen that FhSim significantly overestimates the mean force compared to fishFarm. The reason for the overprediction in FhSim is probably connected to the increased water flow at the net. The Reynolds number prediction is influenced by the increased water flow. Also, the adjustment for local speed up at the twine impacts the load estimation.

The simulated results in currents and waves illustrate the discrepancies obtained in section 7.1.3 for a combined currents and wave condition. Based on the observations for both system A and system B, it is seen that FhSim overestimate mean loads in current and waves. Especially for current velocity U=0.7 m/s, FhSim overpredicts the mean load significantly for both the studied wave steepnesses. The overestimation must be accounted for when applying FhSim in the assessment of mooring line design.

# Chapter 8

# Conclusion

The intention of the work in this thesis has been to evaluate whether the numerical code, FhSim, is able to compute reliable mooring line loads of a gravity net cage in large currents and waves. In order to avoid rupture and subsequent fish escape, mooring lines must be designed according to the global loads. Two gravity net cage systems were subjects to the analysis of mean mooring line load.

## 8.1 Experimental results

The analysis of the experimental results of a complete gravity net cage in current and irregular waves showed that:

- The current force dominated the mean load in an environmental condition of waves and current.
- The mean load could be separated into a mean static load and a mean dynamic load, where the mean dynamic load was assumed to be caused by both waves and currents.
- The mean dynamic load was observed to increase linearly with wave length for a constant wave steepness.
- The mean dynamic load was normalized with the quadratic relative velocity between wave velocity and current velocity $(\frac{u_w}{U_\infty})^2$, and a con-

stant value was found. The constant value showed a current velocity dependency. This normalization indicated that the mean dynamic force might be proportional to $\propto \omega^2 {\zeta_a}^2$.

- Alternative scales for the mean dynamic load was found to be ${\zeta_a}^2$ and ${\zeta_a}^3$, where the first was indicated to be a preferred choice.

## 8.2 Validation of FhSim

The set of experimental results in regular waves and current of the complete gravity net cage was compared to simulations in FhSim. Based on the 6 environmental conditions, the coherence to FhSim was examined. The comparison study showed:

- For current only condition and also for the combined currents and waves, it was observed that FhSim overestimated the mean loads compared to the experiments.
- The discrepancies between the predicted mean loads in FhSim and the experimental results were found to vary between 22%-63%
- From repeated simulations of the identical input file in FhSim, a numerical uncertainty in the solver was detected for this model. The results showed inconsistency in the computation of mean force for this particular model.

Due to a rather limited set of experimental results, and uncertainties connected to both the experimental and the predicted results, it was decided to continue the comparison study with a simplified gravity net cage model. The analysis in FhSim and fishFarm, and also evaluated against existing experimental results showed:

- For the current only condition with current velocity up to U=0.5m/s, a satisfactory agreement between FhSim and experimental results as well as results from fishFarm was observed.
- For the current only conditions with velocity of U=0.7m/s and U=1.0m/s, FhSim overpredicted the mean loads compared to the experimental results.

- In a combination of current and waves with the current velocity U=0.5m/s and waves with steepness H/$\lambda$=1/30, the computed results from FhSim agreed fairly good with results from fishFarm.
- For steeper waves, characterised by the wave steepness H/$\lambda$=1/15 and the current velocities U=0.5m/s and U=0.7m/s, the mean loads from FhSim were significantly overestimated compared to results in fishFarm. The mean mooring line load from FhSim was observed to deviate increasingly compared to fishFarm with increased wave length and wave height. The deviations between FhSim and fish farm was observed for large water flow velocities, and might be explained by the implemented Morison type load model in FhSim.

The results from the study of mean loads of the two gravity net cage systems, indicated that FhSim predicted satisfactory mean load results for current velocities up to U=0.5m/s and waves with steepness of H/$\lambda$=1/30. In an environmental condition with a combination of steeper waves and currents, FhSim was observed to significantly overestimate the mean loads.

For the complete mooring line system, repeated simulations indicated an error in the numerical solver due to the inconsistency in the mean load computations. The discrepancy between simulated and experimental results is found to be up to 60% for the realistic gravity net cage with mooring line system (system A). The numerical results from the simplified mooring system were more reliable.

The validation study was attempted to quantify the level of agreement between experimental data and model prediction. Due to a rather limited set of analysed experimental results, the presented work can be considered as a comparison study between FhSim, experimental results and fishFarm. The described and analysed experiment was not intended as validation data. Experiments with the purpose of generating validation data, should among other factors, carefully ensure high quality data, reduce systematic errors and assure a satisfactory repeatability of the tests.

For a numerical code, assessment of accurate and reliable load computations are required. To ensure margins of the mooring line design, safety factors could be added in the design process. When applying FhSim in an environmental condition with current velocity above U=0.5m/s and steep waves, one should be aware of the possible overprediction of mean mooring line loads.

# Chapter 9

# Further work

The work has focused on mean loads. To design the mooring lines properly, the total force must be evaluated. A transfer function for the total loads could be determined from experiments and compared to the numerical predictions.

The pretension in the mooring lines was observed to alter the load distribution of the mooring system and might also have impacted the floater motions and global forces. In order to examine the effect from pretension on global load estimation, a study of the gravity net cage with different mooring line properties can be performed.

From the experimental results in irregular waves and currents, it was found that the mean dynamic force could be normalized to the quadratic ratio of wave velocity to current velocity or to the squared wave amplitude. To evaluate whether the correlation is valid for other cases, these normalization parameters could be investigated for other net cage models and environmental conditions.

The validation study of FhSim have indicated an overestimation of mean load computation for large current velocities and waves. However, there are uncertainties in the net cage model. It is suggested to detect the possible structural errors, e.g. by including springs in the mooring lines. A comparative study of FhSim for a gravity net cage could be performed, possibly for an even wider range of environmental conditions.

It is suggested to perform a systematic and extensive experimental test that

can form the basis for a comparison study of the load prediction in the numerical codes. A realistic gravity net cage with a complete mooring line system adjusted to a towing tank experiment should be considered. The setup is suggested to be designed in order to measure the global loads and floater motions. Instrumentation for force measurements should be installed in all the mooring lines. Floater collar motions should be monitored at several points around the circumference, but at least in front and aft of the floater. Also the bottom ring motions would be of interest to measure. A mooring line configuration with realistic and symmetric pretension must be ensured. Waves are suggested to be monitored at appropriate positions in front of and to the side of the gravity net cage, and also in connection to where floater motions are measured. To ensure a constant current, it is preferred to execute the test in a towing tank. Environmental loads are suggested to be both waves only, current and waves, and waves only. Both irregular and regular waves are suggested. In particular, the environmental conditions could be current velocities in the range 0.5m/s-1.0m/s and waves characterized by a steepness between $H/\lambda$=1/30-1/15.

# Bibliography


Blevins, R. (2003), *Applied Fluid Dynamics Handbook*, Krieger Publishing Company.

Endresen, P. (2011), Vertical wave loads and response of a floating fish farm with circular collar, Master thesis, Norwegian University of Science.

Endresen, P. (2013), 'Personal communication', SINTEF Fisheries and Aquastructures.

Endresen, P., Birkevold, J., Føre, M., Fredheim, A., Kristiansen, D. & Lader, P. (2014), Draft: Simulation and validation of a numerical nodel of a full aquaculture net cage system. preprint (2014).

Enerhaug, B., Føre, M., Endresen, P., Madsen, N. & Hansen, K. (2012), Current loads on net panels with rhombic meshes, *in* 'Proceedings of the International Conference on Offshore Mechanics and Arctic Engineering - OMAE', pp. 49–60.

Faltinsen, O. (2011), Hydrodynamic aspects of a floating fish farm with circular collar, *in* 'International Workshop on Water Waves and Floating Bodies'.

Faltinsen, O., ed. (1990), *Chapter 5*, Cambridge University Press.

Grue, J. (2014), 'Personal communication', University of Oslo.

Huang, C.-C., Tang, H.-J. & Liu, J.-Y. (2008), 'Effects of waves and currents on gravity-type cages in the open sea', *Aquacultural Engineering* **38**, 105–116.

Jensen, Ø. (2006), Faglig underlag for krav til flytende oppdrettsanlegg

- ns 9415 oppsummeringsrapport, Technical report, SINTEF Fiskeri og havbruk AS.

Jensen, Ø., Dempster, T., Thorstad, E., Uglem, I. & Fredheim, A. (2006), 'Escapes of fishes from norwegian sea-cage aquaculture: causes, consequences and prevention', *Aquaculture Environment Interactions* **1**, 2010.

Klebert, P., Lader, P., Gansel, L. & Oppedal, F. (2013), 'Hydrodynamic interactions on net panel and aquaculture fish cages: A review', *Ocean Engineering* **58**, 260–274.

Kristiansen, D. (2008), Wave Induced Effects on Floaters of Aquaculture Plants, PhD thesis, Norwegian University of Science and Technology.

Kristiansen, T. (2014), 'Personal communication', MARINTEK - SINTEF.

Kristiansen, T. & Faltinsen, O. (2012*a*), 'Modelling of current loads on aquaculture net cages', *Journal of Fluids and Structures* **34**, 218–235.

Kristiansen, T. & Faltinsen, O. (2012*b*), Mooring loads of a circular net cage with elastic floater in waves and current, *in* 'Proceedings of the 6th International Conference on Hydroelasticity in Marine Technology', pp. 183–191.

Kristiansen, T. & Faltinsen, O. (2014), Experimental and numerical study of an aquaculture net cage with floater in waves and current. preprint (2014).

Lader, P. & Fredheim, A. (2006), 'Dynamic properties of a flexible net sheet in waves and current - a numerical approach', *Aquacultural Engineering* **35**, 228–238.

Larsen, C., ed. (1990), *3. Hydrodynamic forces, p. 3.11*, NTNU, Oxford.

Li, P. & Faltinsen, O. (2012), Wave-induced vertical response of an elastic circuar collar of a floating fish farm, *in* 'Proceedings of the 10th International Conference on Hydrodynamics'.

Løland, G. (1991), Current Forces on and Flow through Fish Farms, PhD thesis, Norwegian University of Science and Technology.

Løland, G. (1993), 'Current forces on, and water flow through and around, floating fish farms', *Aquaculture international* **1**, 72–89.

Marichal, D. (2003), Cod-end numerical study, *in* '3rd International Conference on Hydroelasticity in Marine Technology'.

Moe, H., Fredheim, A. & Hopperstad, O. (2010), 'Structural analysis of aquaculture net cages in current', *Journal of Fluids and Structures* **26**, 503–516.

Nygaard, I. (2013), Merdforsøk. kapasitets-tester, Technical report, Norsk Marinteknisk Forskningsinstitutt AS.

Priour, D. (1999), 'Calculation of net shapes by the finite element method with triangular elements', *Communications in Numerical Methods in Engineering* **15**, 757–765.

Reite, K.-J., Føre, M., Aarsæther, K. G., Jensen, J., Rundtorp, P., Kyllingstad, L., Endresen, P., Kristiansen, D., Johansen, V. & Fredheim, A. (2014), Draft: Fhsim - time domain simulation of marine systems. preprint (2014).

Shainee, M., Ellingsen, H., Leira, B. & Fredheim, A. (2013), 'Design theory in offshore fish cage designing', *Aquaculture* **392-395**, 134–141.

Standard, N. (2009), *Marine fish farms. Requirements for site survey, risk analyses, design, dimensioning, production, installation and operation.*

Steen, S. (2012), 'Experimental methods in marine hydrodynamics', Department of Marine Technology.

Steen, S. (2014), 'Personal communication', Norwegian University of Science and Technology.

Thacker, B., Doebling S.W.and Hemez, F., Anderson, M.C., Pepin, J. & Rodriguez, E. (2004), *Concepts of Model Verification and Validation.*

Tsukrov, I., Eroshkin, O., Fredriksson, D., Swift, M. & Celikkol, B. (2003), 'Finite element modeling of net panels using a consistent net element', *Ocean Engineering* **30**, 251–270.

Xu, T.-J., Zhao, Y.-P., Dong, G.-H. & Bi, C.-W. (2013), 'Fatigue analysis of mooring system for net cage under random loads', *Aquacultural Engineering* .

Zhao, Y., Xu, T. & Bi, C. (2012), 'The numerical simulation of hydrodynamics of a fishing net cage', *Hydrodynamics - Theory and Model* .

# Appendix A

# Theory details

## A.1 Force coefficients of a screen model

The theory is developed by (Kristiansen & Faltinsen 2012*a*). For angle of attack $0 < \theta < \frac{\pi}{2}$ the force coefficients can be expressed: (Kristiansen & Faltinsen 2012*a*)

$$\begin{aligned} C_D &= C_N \cos\theta + C_T \sin\theta \\ C_L &= C_N \sin\theta - C_T \cos\theta \end{aligned} \tag{A.1}$$

The force coefficients are expressed separately for small angles of attack $0 < \theta < \frac{\pi}{4}$ and large angles of attack $\frac{\pi}{4} < \theta < \frac{\pi}{2}$.

### A.1.1 Angle of attack $0 < \theta < \frac{\pi}{4}$

Normal and tangential force coefficients are suggested by Kristiansen & Faltinsen (2012*a*):

$$\begin{aligned} C_N(\theta) &= \frac{C_D^{circ.cyl.} Sn(2 - Sn)}{2(1 - Sn)^2},\ 0 \leq \theta \leq \frac{\pi}{4} \\ \frac{C_T(\theta)}{\theta} &= \frac{4C_N(\theta)}{8 + C_N(\theta)},\ 0 \leq \theta \leq \frac{\pi}{4} \end{aligned} \tag{A.2}$$

where $C_D^{circ.cyl.}$ is the Reynolds number dependent drag coefficient of a circular cylinder, based on experimental data from Goldstein (1965).

$$\begin{aligned} C_D^{circ.cyl.} &= -78.46675 + 254.73873(\log_{10} Rn) - 327.8864(\log_{10} Rn)^2 \\ &+ 223.64577(\log_{10} Rn)^3 - 87.92243(\log_{10} Rn)^4 + 20.00769(\log_{10} Rn)^5 \\ &- 2.44894(\log_{10} Rn)^6 + 0.12479(\log_{10} Rn)^7 \end{aligned} \tag{A.3}$$

Equation (A.3) can be applied for $10^{\frac{3}{2}} \leq Rn \leq 10^4$ where Rn is defined as in A.4 with $U_{rel}$ as the maximum value of relative velocity (Kristiansen & Faltinsen 2012*a*).

$$Re = \frac{U_{rel} d_w}{\nu(1 - Sn)} \tag{A.4}$$

### A.1.2 Angle of attack $\frac{\pi}{4} < \theta < \frac{\pi}{2}$

In this interval, $C_T(\theta)$ and $C_N(\theta)$ must be generalized. Kristiansen & Faltinsen (2012*a*) have proposed expressions for drag and lift coefficients as follows:

$$\begin{aligned} C_D(\theta) &= c_d \cos\theta,\ 0 < \theta < \frac{\pi}{2} \\ C_L(\theta) &= c_l \sin 2\theta,\ 0 < \theta < \frac{\pi}{2} \end{aligned} \tag{A.5}$$

where $c_d = C_N(0)$ calculated from A.2 when $\theta = 0$, $c_l = C_N(\frac{\pi}{4})\sin(\frac{\pi}{4}) - C_T(\frac{\pi}{4})cos(\frac{\pi}{4})$ and is calculated from A.2 when $\theta = \frac{\pi}{4}$.

# Appendix B

# Scaling laws

The physical quantities of the model are assumed to be Froude scaled as presented in equation (B.1). Geometrical similarity as in equation B.2 is also assumed.

$$\frac{U_M}{\sqrt{gL_M}} = \frac{U_F}{\sqrt{gL_F}} \tag{B.1}$$

$$\lambda = \frac{L_F}{L_M} \tag{B.2}$$

where $U_M$ is the velocity in model scale, $L_M$ is the geometric length in model scale, $U_F$ is the velocity in full scale, $L_F$ is the geometric length in full scale and $\lambda$ is the scaling factor.

Table B.1 gives and overview of the derived scaling factors for the different parameters.

Table B.1: Scaling ratios

| Description | Scaling factor | Unit |
|---|---|---|
| Length | $\lambda$ | m |
| Velocity | $\sqrt{\lambda}$ | m/s |
| Time | $\sqrt{\lambda}$ | s |
| Acceleration | 1 | $m/s^2$ |
| Force | $\lambda^3$ | N |
| Moment | $\lambda^4$ | Nm |
| Structural mass | $\lambda^3$ | kg |
| Angle | 1 | deg/s |
| Angular velocity | $\frac{1}{\sqrt{\lambda}}$ | deg |

# Appendix C

# Plots of slow drift force

## C.1 Variation of upper cut-off frequency, $f_u$

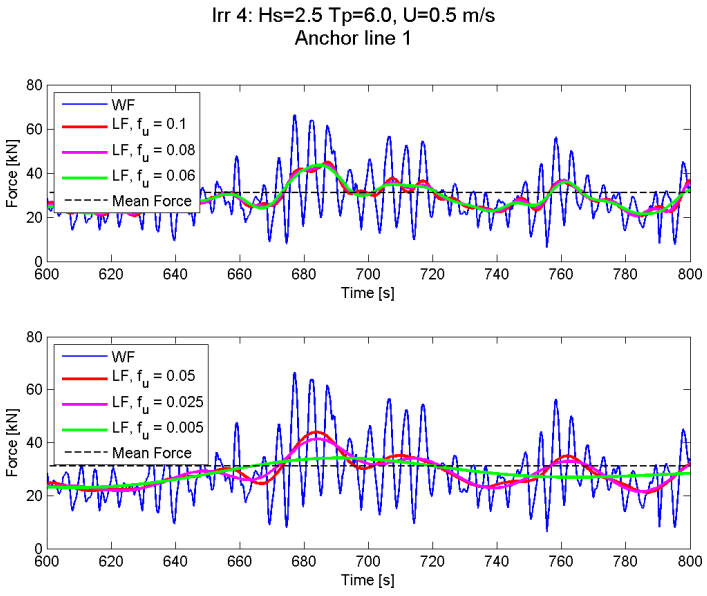


Figure C.1: Total force (WF), low frequency force (LF) and mean force, $f_u$ varied

Table C.1: Variation of upper cut-off frequency, $f_u$, and impact on standard deviation, $\sigma$, for LF force. $\beta$ is kept constant to 0.005

| Parameter | | | | | | |
|---|---|---|---|---|---|---|
| $f_u$ [1/s] | 0.1500 | 0.1000 | 0.0500 | 0.0100 | 0.0050 | 0.0025 |
| LF force $\sigma$ | 7.12 | 6.34 | 6.06 | 4.41 | 3.37 | 2.82 |

## C.2 Variation of $\beta$

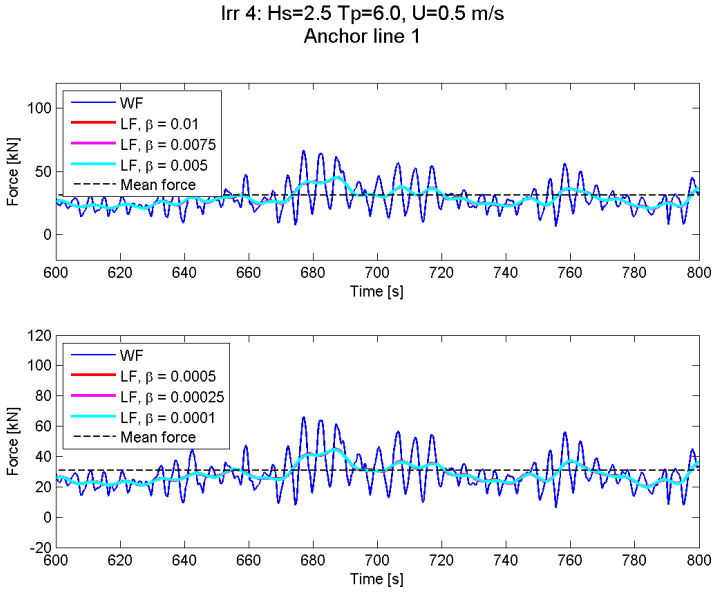


Figure C.2: Total force (WF), low frequency force (LF) and mean force, $\beta$ varied

Table C.2: Variation of $\beta$, and impact on standard deviation, $\sigma$, for LF force. $f_u$ is kept constant to 0.01

| Parameter | | | | | | |
|---|---|---|---|---|---|---|
| $\beta$ | 0.0100 | 0.0075 | 0.0050 | 0.0005 | 0.0003 | 0.0001 |
| LF force $\sigma$ | 6.37 | 6.36 | 6.34 | 6.30 | 6.29 | 6.29 |

# Appendix D

# Check of simulated results in FhSim, system A

Due to quite large deviations in post processed results, it is of interest to validate the post processing procedure applied in this work for the csv-file. When this is clarified, simulations of the same case will be repeated in order to detect errors in the deviating results.

## D.1 Check of post processing routine

To perform this, the output-files from the simulations in Endresen et al. (2014) will be postprocessed with the author's matlab-scripts. Further, the same input-files as used for the simulations in the draft article will be used for simulations.

Table D.1 presents the mean forces read from (Endresen et al. 2014) (P) and the present computations (Num) based on csv.files from Endresen (2013). The pretension is subtracted in the W1 and W2 case.

Table D.1: Mean force [kN], post processing routine check

| | Average bridles | | | Buoy chain | | | Anchor line | | |
|---|---|---|---|---|---|---|---|---|---|
| | P | Num | % | P | Num | % | P | Num | % |
| C1 | 32.0 | 31.1 | -2.7 | 22.0 | 20.8 | -5.6 | 52.0 | 52.9 | 1.7 |
| C2 | 44.0 | 43.2 | -1.7 | 28.0 | 28.0 | 0.0 | 75.0 | 77.0 | 2.6 |
| W1 | 3.8 | 3.6 | -2.7 | 3.8 | 3.4 | -11.2 | 8.0 | 7.9 | -1.3 |
| W2 | 1.9 | 1.9 | 1.8 | 3.2 | 2.7 | -15.3 | 5.9 | 6.1 | 2.7 |

By processing received .csv-file and applying the present postprocessing routing, similar results as Endresen et al. (2014) is obtained.

## D.2 Reproducing draft article results

The computed ensemble average of 6 simulation are compared to results in Endresen et al. (2014). In table D.2, $\overline{X}$ is compared to the results in Endresen et al. (2014), denoted Num. Note that the pretension is only subtracted for W1 and W2. The coherence between simulated mean force is examined. It is observed that $\overline{X}$ in general is underestimated compared to Num. The underestimation varies in the range $15\% - 40\%$.

Table D.2: Ensemble average of mean force [kN] for simulations 1-6 compared to results in Endresen et al. (2014).

| | Average bridles | | | Buoy chain | | | Anchor line | | |
|---|---|---|---|---|---|---|---|---|---|
| | Num | $\overline{X}$ | % | Num | $\overline{X}$ | % | Num | $\overline{X}$ | % |
| C1 | 31.1 | 19.8 | -36.4 | 20.8 | 15.2 | -26.6 | 52.9 | 36.2 | -31.5 |
| C2 | 43.2 | 33.4 | -22.7 | 28.0 | 23.7 | -15.4 | 77.0 | 62.6 | -18.7 |
| W1 | 3.6 | 2.4 | -33.1 | 3.3 | 3.2 | -3.6 | 7.9 | 6.2 | -21.6 |
| W2 | 1.9 | 0.9 | -52.5 | 2.7 | 2.8 | 5.3 | 6.0 | 4.8 | -20.1 |

The results from simulations of system A, do not indicate an agreement between the performed simulated results and the results presented in (Endresen et al. 2014).

## D.3 Time series plots of the force from simulations of system A

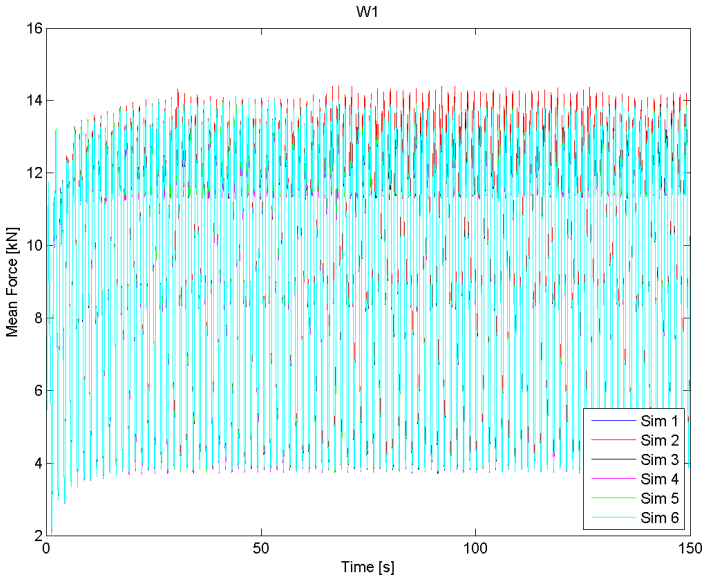


(a) Force in anchor line, W1

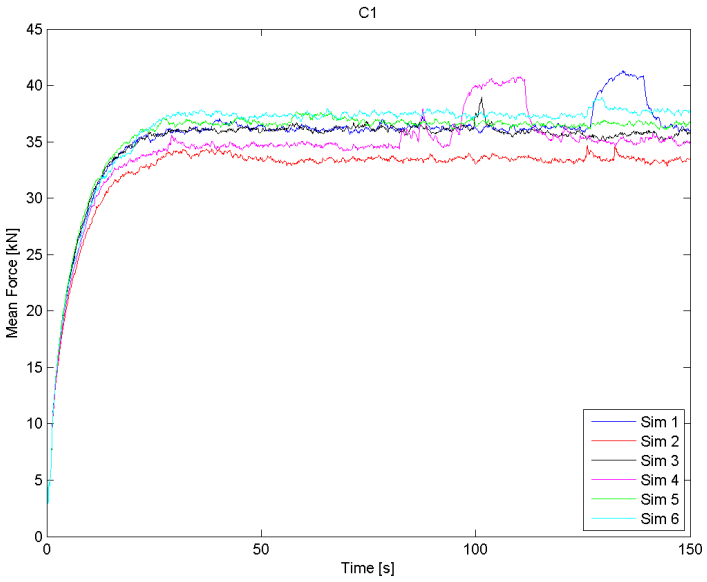


(b) Force in anchor line, C1



Figure D.1: Time series of force in anchor line. Waves only (W1) and current only (C1)

# Appendix E

# Mean dynamic load

## E.1 Dynamic mean force and relative velocity

The dynamic mean force is normalized with $(\frac{u_w}{U})^2$ in a similar way as presented in section 6.2.2, point 2.

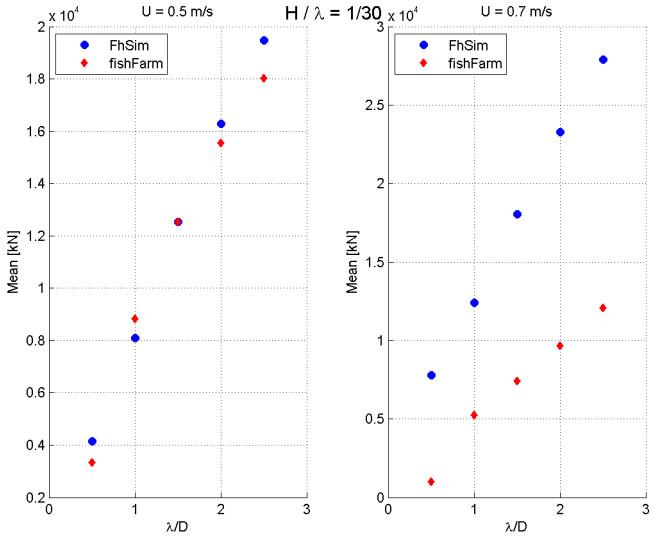


Figure E.1: Mean force subtracted current only force ($F_{DYN}$)[kN], normalized with $(\frac{u_w}{U})^2$

## E.2 Scaling the mean dynamic load as added drag

As presented in section 6.2.2, the dynamic force is scaled as added drag. The results are presented in figure E.2 and E.3.

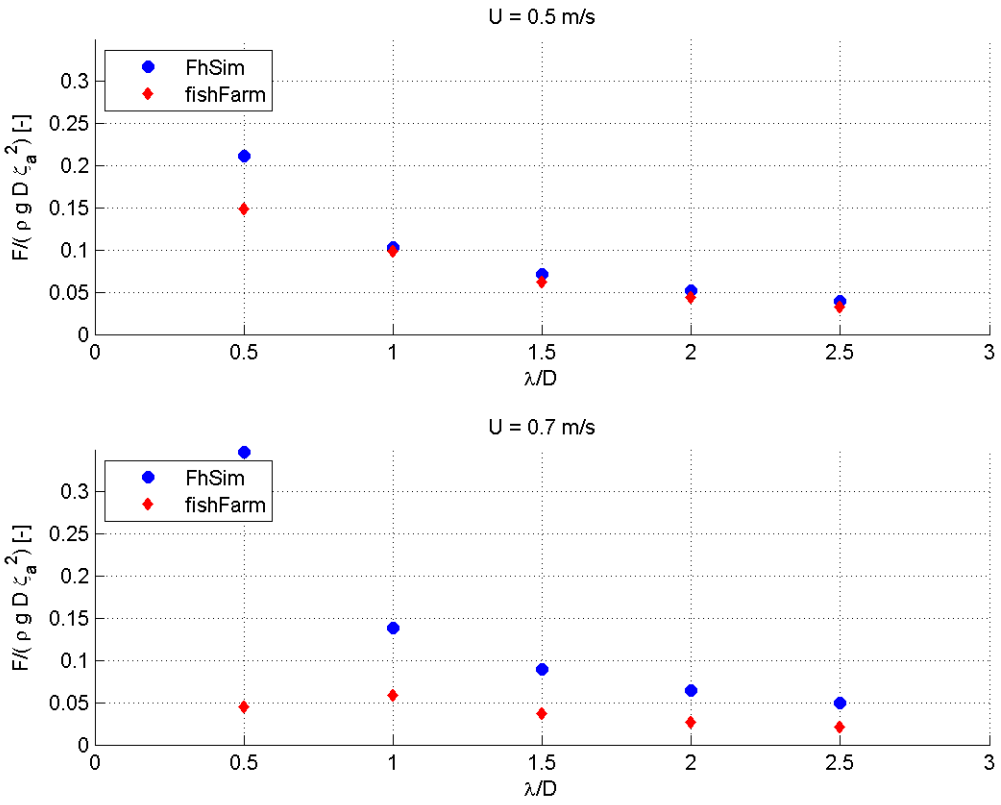


Figure E.2: Added drag from simulations in FhSim and fishFarm. $H/\lambda = 1/30$

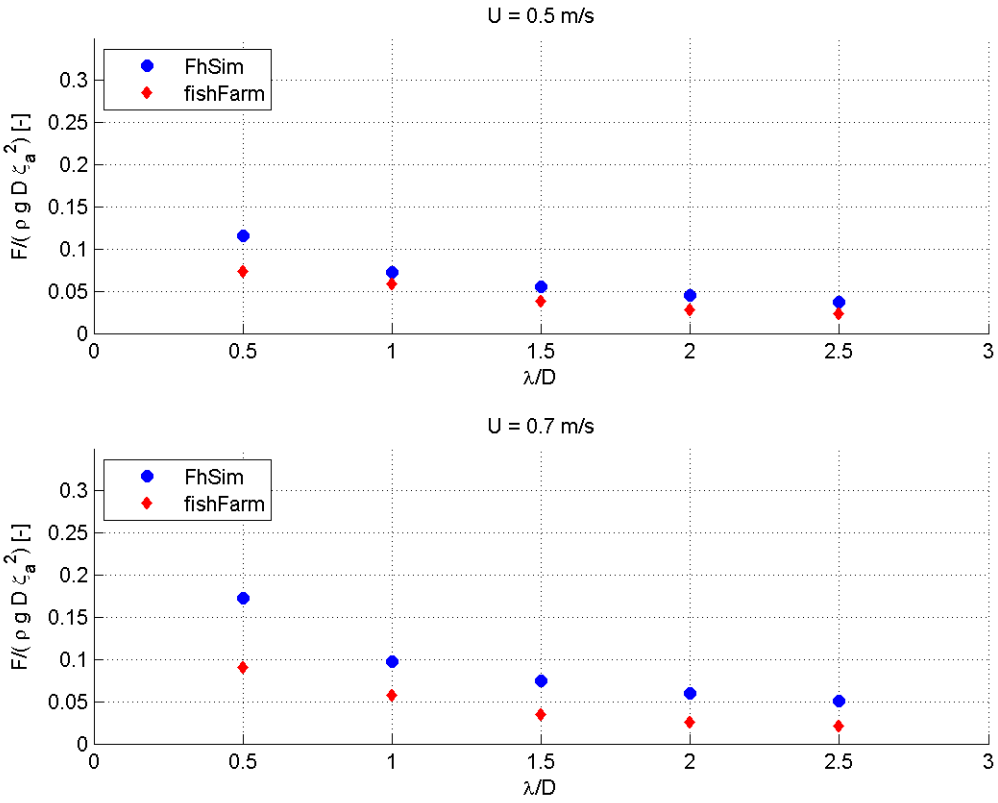


Figure E.3: Added drag from simulations in FhSim and fishFarm. $H/\lambda = 1/15$